

NPS72-87-003CR

NAVAL POSTGRADUATE SCHOOL

Monterey, California



CONTRACTOR REPORT

AMBIENT SCATTERING FROM RING-SYMMETRIC
SPACECRAFT EXHAUST PLUME

by

- Joseph Falcovitz

April 1987

Approved for public release; distribution unlimited.

Prepared for: Strategic Defense Initiative Office
The Pentagon
Washington, DC 20301-7100

FedLocs
D 202.1412:
NPS-72-82-003 CR

NAVAL POSTGRADUATE SCHOOL
Monterey, California

RADM R. C. Austin
Superintendent

D. A. Schrady
Provost

The work reported herein was performed for the Naval Postgraduate School by Dr. Joseph Falcovitz under contract N00228-87-C-3046. The work presented in this report is in support of "Rarefied Gas Dynamics of Laser Exhaust Plume" sponsored by the Strategic Defense Initiative Office/Directed Energy Office. This is the final report for that contract. The work provides information concerning scattering of exhaust molecules by ambient air and effects on spacecraft charging. The project at the Naval Postgraduate School is under the cognizance of Distinguished Professor A. E. Fuhs who is principal investigator.

Reproduction of all or part of this report is authorized.

Prepared by:

REPORT DOCUMENTATION PAGE

EPORT SECURITY CLASSIFICATION CLASSIFIED		1b RESTRICTIVE MARKINGS NONE	
SECURITY CLASSIFICATION AUTHORITY		3. DISTRIBUTION/AVAILABILITY OF REPORT Approved for Public Release; Distribution Unlimited	
ECLASSIFICATION/DOWNGRADING SCHEDULE			
RFORMING ORGANIZATION REPORT NUMBER(S) 672-87-003CR		5. MONITORING ORGANIZATION REPORT NUMBER(S) NPS72-87-003CR	
NAME OF PERFORMING ORGANIZATION SEPH FALCOVITZ	6b. OFFICE SYMBOL <i>(If applicable)</i> Code 72	7a. NAME OF MONITORING ORGANIZATION NAVAL POSTGRADUATE SCHOOL, CODE 72	
ADDRESS (City, State, and ZIP Code) search Contractor val Postgraduate School ntersey, CA 93943-5100		7b. ADDRESS (City, State, and ZIP Code) Space Systems Academic Group Monterey, CA 93943-5100	
NAME OF FUNDING/SPONSORING ORGANIZATION Strategic Defense Initiative Office	8b. OFFICE SYMBOL <i>(If applicable)</i> SDIO/DEO	9. PROCUREMENT INSTRUMENT IDENTIFICATION NUMBER	
ADDRESS (City, State, and ZIP Code) 10/DEO shington, DC 20301-7100		10. SOURCE OF FUNDING NUMBERS	
		PROGRAM ELEMENT NO.	PROJECT NO.
		TASK NO.	WORK UNIT ACCESSION NO.

TITLE (Include Security Classification)

BIENT SCATTERING FROM RING-SYMMETRIC SPACECRAFT EXHAUST PLUME

PERSONAL AUTHOR(S)

SEPH FALCOVITZ

TYPE OF REPORT Contractor Report	13b TIME COVERED FROM JAN 87 TO MAR 87	14. DATE OF REPORT (Year, Month, Day) April 1987	15 PAGE COUNT 60
--------------------------------------------	--------------------------------------------------	------------------------------------------------------------	----------------------------

SUPPLEMENTARY NOTATION

COSATI CODES			18 SUBJECT TERMS (Continue on reverse if necessary and identify by block number)
FIELD	GROUP	SUB-GROUP	
			Spacecraft Contamination, Exhaust Plume, Ambient Scattering, First-Collision

ABSTRACT (Continue on reverse if necessary and identify by block number)

present a first-collision model for the evaluation of return flux from the exhaust plume of a ring-symmetric DF laser in LEO, generated by an incident flux of ambient molecules traveling at orbital speed. The steady state is bounded by a pair of lip-centered rarefaction fans, and unless spacecraft attitude enables incident air molecules to reach the plume through the cavitation regions that extend beyond these fans, the spacecraft is shielded from ambient scattering by its own plume. Assuming hard-spheres collisions, the first-collision model is given by a simple closed-form expression that can be regarded as a source term for scattered exhaust molecules. This source term is integrated numerically throughout the fan, yielding the flux arriving at some surface "target". Quantitatively, it is shown that for a typical HF/DF laser exhaust the contamination level generated by ambient scattering is not significant. It was found that the maximum return flux of HF+DF constitutes about 1% of the incident ambient flux; this ratio will be nearly constant for LEO altitudes. The value of this flux ratio is known to be dependent on the molecular collision model; it may change upon replacing the hard-spheres approximation by a more realistic collision model. A possible modification of spacecraft charging by the exhaust was examined, including production of HF⁺ and DF⁺. The only significant effect seemed to be shadowing of the downstream half of the spacecraft at oblique orbital attitudes.

DISTRIBUTION/AVAILABILITY OF ABSTRACT <input checked="" type="checkbox"/> UNCLASSIFIED/UNLIMITED <input type="checkbox"/> SAME AS RPT <input type="checkbox"/> DTIC USERS	21. ABSTRACT SECURITY CLASSIFICATION UNCLASSIFIED
NAME OF RESPONSIBLE INDIVIDUAL JEN E. FUHS, Distinguished Professor	22b. TELEPHONE (Include Area Code) (408) 646-2948

FORM 1473, 84 MAR

83 APR edition may be used until exhausted.

All other editions are obsolete

SECURITY CLASSIFICATION OF THIS PAGE

★ U.S. Government Printing Office: 1986-606-24.

ABSTRACT

We present a first-collision model for the evaluation of return flux from the exhaust plume of a ring-symmetric HF/DF laser in LEO, generated by an incident flux of ambient molecules traveling at orbital speed. The steady plume is bounded by a pair of lip-centered rarefaction fans, and unless spacecraft attitude enables incident air molecules to reach the plume through the cavitation regions that extend beyond these fans, the spacecraft is shielded from ambient scattering by its own plume. Assuming hard-spheres collisions, the first-collision model is given by a simple closed-form expression that can be regarded as a source term for scattered exhaust molecules. This source term is integrated numerically throughout the fan, yielding the flux arriving at some surface "target point". Quantitatively, it is shown that for a typical HF/DF laser exhaust the contamination level generated by ambient scattering is not significant. It was found that the maximum return flux of HF + DF constitutes about 2% of the incident ambient flux; this ratio will be nearly constant for LEO altitudes. The value of this flux ratio is shown to be dependent on the molecular collision model; it may change upon replacing the hard-spheres approximation by a more realistic collision model. A possible modification of spacecraft charging by the exhaust was examined, including production of HF^- and DF^- . The only significant effect seemed to be shadowing of the downstream half of the spacecraft at oblique orbital attitudes.

ACKNOWLEDGEMENTS

This work is part of a study involving gas dynamics of exhaust plumes from spacecrafts. It was conducted under the cognizance of Distinguished Professor Allen E. Fuhs, who initiated this research program at the Naval Postgraduate School. I wish to thank Professor Fuhs for his inspiring guidance and deeply appreciate his continued support.

TABLE OF CONTENTS

1.	INTRODUCTION.....	1
2.	COMPUTATION OF THE PLUME FLOW FIELD.....	4
3.	AMBIENT SCATTERING.....	8
3.1	First Collision Model.....	8
3.2	Flux Integration Scheme.....	10
4.	RESULTS AND DISCUSSION.....	17
5.	SPACECRAFT CHARGING.....	23
6.	CONCLUDING REMARKS.....	27
7.	REFERENCES	29
	APPENDIX A. DESCRIPTION OF AMB CODE.....	31
A.1	Description of Subroutines.....	31
A.2	Listing of AMB code.....	34
8.	DISTRIBUTION LIST	52

LIST OF FIGURES

Figure 1-1.	Ring-Symmetric HF/DF Laser Exhaust Plume	3
Figure 1-2.	Schematic Description of Ambient Scattering. The Cavitation Region is Bounded by Lines CA and CB	3
Figure 2-1.	Power $\delta(0,\beta)$ for the power-law Approximation.....	6
Figure 2-2.	Variation of Mach Number along Characteristic Line $\beta = 13$	7
Figure 3-1.	Incidence-Plane Description of Flux Integration Scheme	14
Figure 3-2.	Hard-Spheres Collision Notation	15
Figure 3-3.	Scattering Envelope for Hard-Spheres Collision.....	16
Figure 4-1.	Variation of Return Flux with Target Point (X_s). Target Point at Incidence-Plane ($\phi_A = 0$) and Constant Incidence-Angle ($\psi_A = 20^\circ$).....	20
Figure 4-2.	Variation of Return Flux with Ambient Incidence Angle (ψ_A). Fixed Target Point ($X_s = 1$ m) Located at Incidence-Plane ($\phi_A = 0$).....	21

Figure 4-3. Variation of Return Flux with Ambient Azimuth Angle (ϕ_A). Fixed Target Point ($X_s = 1$ m) and Ambient Incidence Angle ($\psi_A = 20^\circ$)	22
----------------------------------------------------------------------------------------------------------------------------------------------------------------------------------	----

LIST OF TABLES

Table 4-1. Typical Operating Conditions of HF/DF Laser Exhaust.	19
-------------------------------------------------------------------------	----

EMPTY PAGE

I. INTRODUCTION

This presentation is part of a study on the gas dynamics of ring-symmetric exhaust plumes in space, conducted at the Naval Postgraduate School in Monterey. A ring-symmetric jet has zero thrust, which makes it suitable as an exhaust configuration for various open loop power plants designed to produce high power for relatively short durations. One such system is an envisioned space-based chemical laser, shown schematically in Fig. 1-1. In the case of a chemical laser, a ring-symmetric configuration would also enable the laser radiation to emerge in the form of an axisymmetric beam.

The exhaust nozzle should be designed to bring the outgoing flow to a supersonic speed at the nozzle exit surface. The near field of a free jet is then composed of an inner core bounded by a pair of ring-symmetric rarefaction fans centered at the nozzle lips (Fig. 1-1). Beyond the limiting characteristic surface of the centered rarefaction waves (CRW), a near-vacuum condition prevails. For the purpose of continuum gas dynamic analysis, we assume it is a perfect vacuum.

An earth orbiting vehicle is subject to an oncoming stream of ambient molecules at a speed of $U_A \approx 8$ (km/sec), in a direction depending upon its orientation relative to the orbital velocity vector. This speed is sufficiently high to cause backscattering of exhaust molecules (see schematic description in Fig. 1-2) moving at speeds appropriate to chemical combustion (about 2 to 4 km/s). However, large exhaust plumes, having achieved stationary flow, may be sufficiently dense at their outer fringes to effectively trap and entrain all oncoming ambient molecules. Thus, ambient scattering may be significant only in selected ranges of attitude angles, at which ambient molecules can reach the vicinity of the spacecraft by traveling almost collisionlessly through cavitation regions. Exhaust molecules that may be "candidates" for ambient scattering will hence come from plume segments flanked by cavitation regions. The contribution of ambient scattering to contamination will thus be highly dependent upon spacecraft geometry and orientation. This may well affect spacecraft design and operating procedures.

The purpose of this report is to present a first-collision model for estimating the flux of exhaust molecules backscattered from the fringes of the plume by ambient molecules, along with results of sample flux computations performed on a typical HF/DF laser exhaust configuration. The flow field throughout the plume is assumed to be governed by the equations of continuum gas dynamics. In principle, the flow could be obtained by solving the governing equations, i.e., the equations for stationary isentropic flow in two-dimensional axisymmetric coordinates. In practice, this is normally

accomplished by integrating the flow equations in characteristic form, using some finite difference scheme (method-of-characteristics). We have performed such computations, but given the complexity of applying them to the subsequent integration of ambient scattering flux (due to the need for two-dimensional interpolations from an irregular solution grid), we opted for a different alternative : a closed-form approximation to the ring-symmetric CRW, based on an analytic expression for flow variables along characteristic lines that fan out from the nozzle lip.

The plan of this report is as follows. In Ch. 2 we outline the approximation to the ring-symmetric CRW and present some computation results that demonstrate its accuracy. In Ch. 3 we describe the first-collision model and the 3-D spatial integration scheme for computing the flux arriving at the cylindrical spacecraft. In Ch. 4 some results of backscattered flux of corrosive molecules (HF+DF), showing flux variation with target point location (X_s) and attitude angles (ψ_A, φ_A) are presented. In Ch. 5 we take up the subject of spacecraft charging, using results of ambient scattering to assess the effect of laser exhaust on spacecraft charging. This is followed by concluding remarks in Ch. 6 and a list of references in Ch. 7. A concise description of the flux computation code "AMB" is given in Appendix A, followed by the code listing.

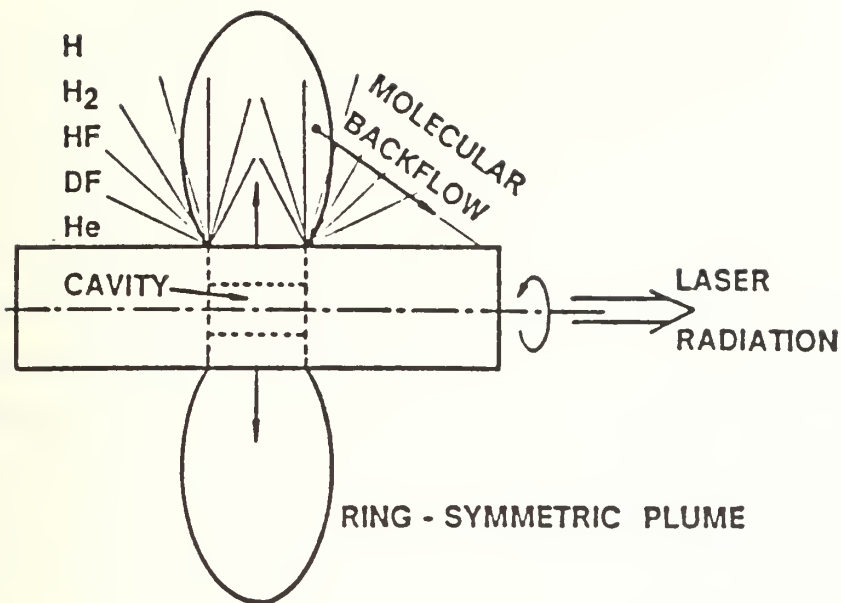


Figure 1-1. Ring-Symmetric HF/DF Laser Exhaust Plume.

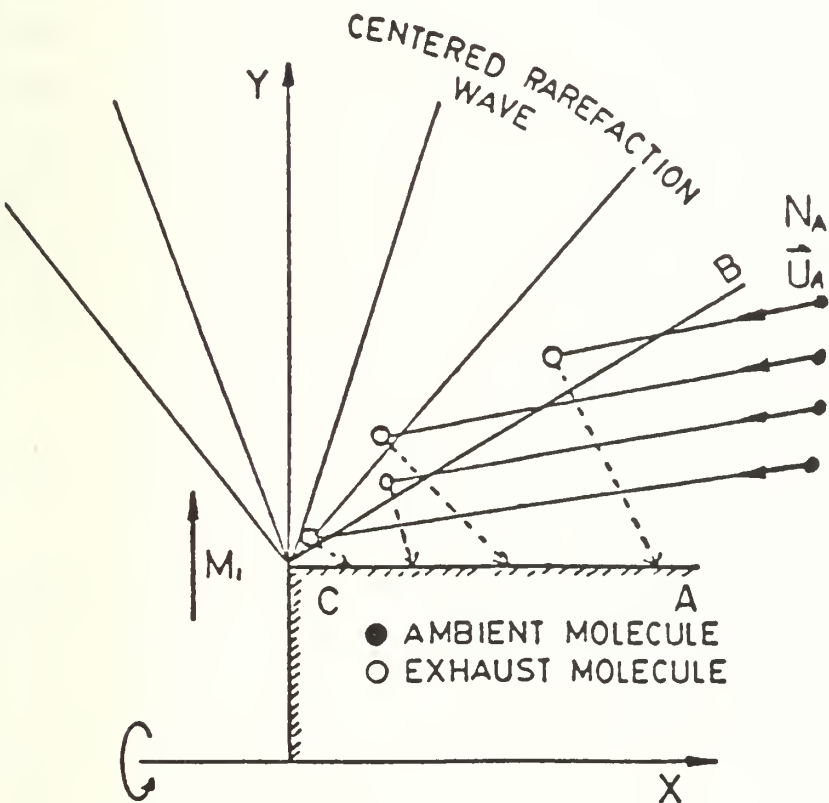


Figure 1-2. Schematic Description of Ambient Scattering. The Cavitation Region is Bounded by Lines CA and CB.

2. COMPUTATION OF THE PLUME FLOW FIELD

Most ambient molecules entering the CRW that flanks the exhaust plume are stopped within several mean free paths from their point of entry. A quantitative estimate of ambient back-scattering would thus depend on the flow field at the outer (hypersonic) fringes of the lip-centered CRW. Even though the flow in those regions is generally past the surface of continuum breakdown, the density there is reasonably well approximated by the continuum flow field, as demonstrated by Bird's Monte-Carlo simulation of a Prandtl-Meyer expansion to vacuum [1]. The evaluation of ambient scattering thus calls for an ancillary computational procedure capable of rendering the continuum flow field at a large number of points in the ring-symmetric CRW of an exhaust plume. This method was described in a recent report [2]. Here we just outline the key ideas and main results of this approximation method.

Our analytic approximation to a ring-symmetric CRW is formulated as follows. In a planar CRW (Prandtl-Meyer flow) all flow variables are uniform along the characteristic lines that fan out from the corner (we assume they are the C^+ family). In the ring-symmetric case the flow near the corner approaches asymptotically a corresponding planar CRW flow, which we term the *associate* CRW. However, the gradients along C^+ characteristics at the corner of a ring-symmetric CRW do not vanish as in a planar CRW. The key idea is thus: evaluate flow gradients in C^+ directions at the corner, then use them to extrapolate the associate CRW along C^+ lines to a finite distance from the corner. The extrapolation is a nonlinear function of the radial coordinate y , chosen so that the ensuing expression conforms exactly to the flow at the leading (exit) characteristic $C^+(\beta_1)$. Omitting all details of the analysis, the resulting approximation is presented as the following power-law :

$$f(\alpha, \beta) = f(0, \beta) [y(\alpha, \beta)/y(0, \beta)]^{\delta(0, \beta)} \quad (2-1)$$

where f is the streamtube area ratio for isentropic flows ($f=1$ at a sonic point), β is the Mach number of a particular characteristic line at the corner, α is a coordinate along the $C^+(\beta)$ characteristic line ($\alpha=0$ at the corner), and y is the radial coordinate of a point on the characteristic line $C^+(\beta)$. The Mach number at point (α, β) is readily determined from $f(\alpha, \beta)$ using the standard relation between area ratio and Mach number [3]. A closed-form expression for $\delta(0, \beta)$ was developed but is not given here; instead, this function is shown in Fig. 2-1. We note that δ approaches the asymptotic value of $2/(3-\gamma)$ as β increases to infinity, and that generally $1 < \delta(0, \beta) < 2$ so that streamtubes diverge at a rate intermediate between that of cylindrical and spherical expansion flows.

Clearly, in an isentropic flow all thermodynamic variables, and in particular density, can be evaluated from \mathbf{f} . This approximation is readily applied to the hypersonic portions of a ring-symmetric CRW since it turns out that characteristic lines are nearly straight there, which means that the characteristic line $C^+(\beta)$ passing through a given point can be readily determined. As a demonstration of the degree of accuracy obtainable from this approximation, we show in Fig. 2-2 the variation of Mach number along a characteristic line in the ring-symmetric CRW, compared with an accurate method-of-characteristics computation. This comparison demonstrates that the analytic approximation is reasonably accurate to nearly ten corner-radii away from the corner.

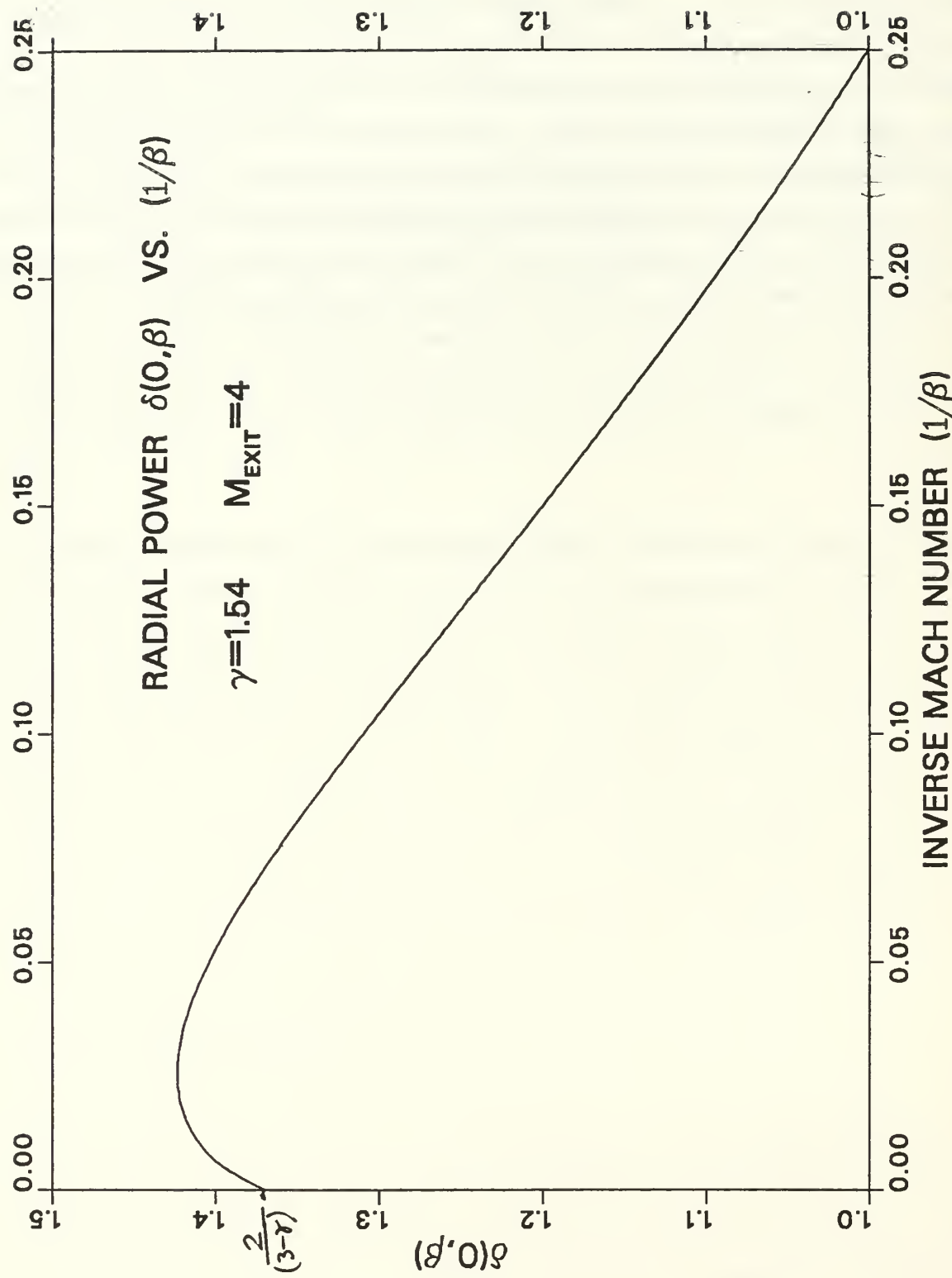


Figure 2-1. Power $\delta(0,\beta)$ for the power-law Approximation.

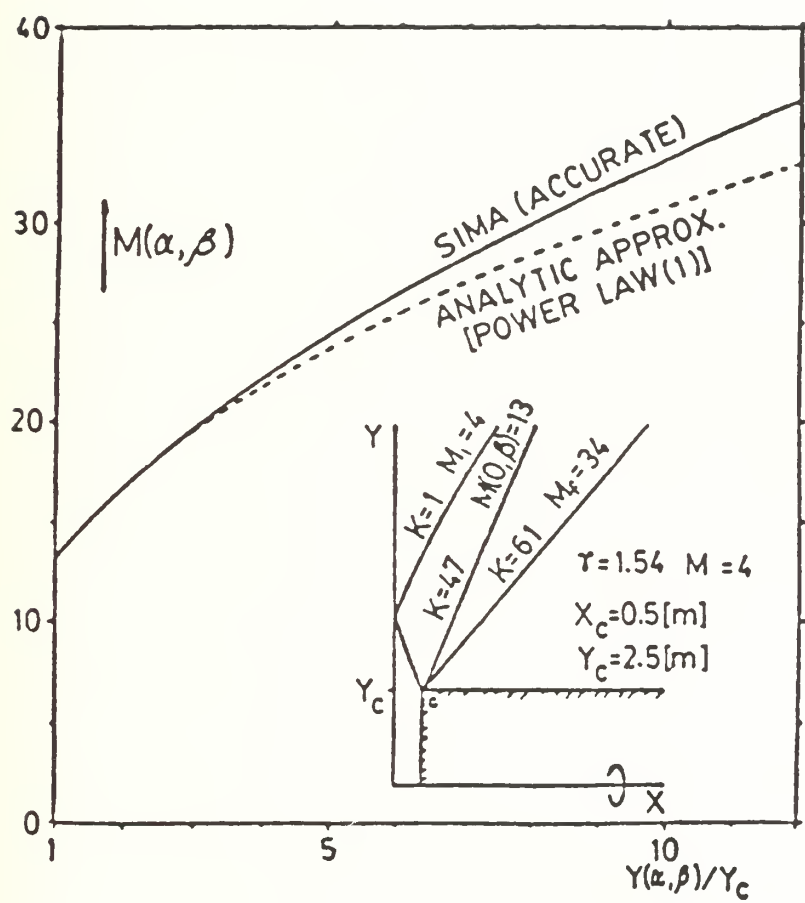


Figure 2-2. Variation of Mach Number along Characteristic Line $\beta = 13$.

3. AMBIENT SCATTERING

When a rocket or laser exhaust is released into space from an earth-orbiting spacecraft, it encounters an oncoming stream of ambient molecules flowing at the orbital speed of $U_A \approx 8$ (km/sec). At altitudes higher than 200 (km), the air/air mean free path exceeds 250 (m), so that it is considerably larger than almost any spacecraft. Consequently, ambient molecules would hardly be subjected to a shock transition prior to their impact at the spacecraft or exhaust plume. In this chapter we describe the formulation of the first-collision model in Section 3.1 and then proceed to present the derivation of the flux integration scheme for hard-sphere collisions in Section 3.2.

3.1 First Collision Model

The highest ambient number density that we consider for earth-orbiting spacecrafts is $N_A = 1 \times 10^{16}$ (m⁻³), which roughly corresponds to Sunspot Maximum at 200 (km) [4]. The typical laser exhaust (Table 4-1) would reach a number density of about 2×10^{19} (m⁻³) at the very high Mach number of 30. Hence, ambient flux constitutes just a slight perturbation to the near-field portion of a typical laser exhaust plume. Obviously, ambient molecules that penetrate the plume, would subsequently be entrained by the main flow. But how far do they penetrate? And would exhaust molecules scattered by them reach the spacecraft? In seeking answers to these questions, we are led to some interesting observations concerning ambient scattering.

Consider the HF laser depicted in Fig. 1-1. The spacecraft diameter is 5 (m) and the centrally located ring-symmetric nozzle is 1 (m) wide. Typical operating conditions (Table 4-1) are assumed. They are based on some experimental HF/DF laser studies conducted at TRW [5,6]. Suppose that the spacecraft axis is normal to the orbital velocity vector (normal incidence). Let the plane of incidence be the plane defined by the intersection of the spacecraft axis with the orbital velocity vector. The probability that an ambient molecule traveling in the plane of incidence would reach the spacecraft collisionlessly is $\exp(-\eta)$, where η is its expected number of collisions with exhaust molecules. We define the number η as "molecular thickness", in analogy to "optical thickness". So in order to determine the extent to which ambient molecules at normal incidence reach the spacecraft, we seek the distribution of radial molecular thickness as function of distance from the spacecraft mid-plane (normal to axis at its midpoint).

For this purpose we computed the ring-symmetric exhaust flow field, using a semi-inverse marching characteristics scheme [7]. The marching was in the radial direction, starting with uniform flow at the nozzle exit; the computation was carried on until it became evident that even at a distance of 20 (m) from the mid-plane, the radial molecular thickness was well over 40. The entire spacecraft was thus shielded from any ambient scattering at (or near) normal incidence. This shielding effect has two significant implications which we discuss briefly below.

- (a) It is present only during stationary exhaust flow. At startup and shutdown phases, ambient scattering may be substantial even at normal incidence.
- (b) During the stationary phase, ambient scattering is substantial only at attitude angles that enable ambient molecules to reach the vicinity of the plume by traveling through "molecularly thin" cavitation regions that flank the plume. We thus anticipate a decisive dependence of ambient scattering on attitude variations, whenever those variations steer the spacecraft into or out of a shielded posture.

As a first attempt at a quantitative estimate of ambient scattering flux, we have formulated a simple first-collision model of this effect. In the sequel we present an outline of the model, along with some sample results evaluated for an HF laser configuration identical to that considered for the shielding effect mentioned above.

The basic idea is the following. Ambient molecules entering an exhaust plume, require several collisions to become fully "accommodated" with the main flow (i.e., to be entrained by the main flow at the prevailing flow velocity and temperature). One may reasonably approximate this process by considering just one collision - the first.

With the help of some additional assumptions, we were able to derive a closed form expression for the flux of exhaust molecules that arrive at the spacecraft following a first collision with an ambient molecule. The main assumptions of this model are :

- (1) **FIRST COLLISIONS:** Only first collisions for either ambient or exhaust molecules are considered. Hard-spheres elastic collisions are assumed. Upon a second collision of either an ambient or an exhaust molecule, it is considered "lost" (i.e., it joins the main flow). Collisions of ambient molecules with spacecraft surfaces are ignored. Ambient molecules are assumed to traverse cavitation regions collisionlessly.

- (2) COLD FLOW: The oncoming ambient air flow is deemed "cold"; i.e., all molecules move at the uniform orbital velocity. The same "cold" assumption is applied to the exhaust flow, since most ambient scattering takes place at plume regions of very high Mach numbers (well over 10, in the present case).
- (3) CRW Flow Field: ring-symmetric CRW flow field is determined from the power-law approximation described in Ch. 2 above. This approximation approaches Prandtl-Meyer flow at points whose distance from the nozzle lip is much smaller than the spacecraft radius.

Based on these assumptions, ambient scattering is represented as a source term for side-scattered exhaust molecules, distributed throughout the lip-centered rarefaction fan. The total flux arriving at a specified point on the cylindrical spacecraft is readily computed by integrating numerically that source distribution over the entire ring-fan.

The highlights of the spatial integration scheme (Fig. 3-1) are as follows. The limiting characteristic surface ($M = \infty$) of the ring-symmetric CRW is divided into surface elements formed by dividing the surface into a set of ring-strips which are subdivided in the circumferential (azimuthal) direction (ϕ) into surface elements. The line-of-sight ($\vec{\Omega}$) from the "target point" on the spacecraft to the center of each surface element is extended into the ring-symmetric CRW, and flux integration using the first-collision source term with appropriate weight factors is performed along this line until convergence is attained. Contributions from each surface element are summed, taking care to disregard portions of the ring-symmetric CRW that are shadowed by the cylindrical spacecraft (either the line-of-sight or the trajectory of oncoming ambient molecules may be shadowed). Some further details of the flux integration scheme and hard-spheres collisions are provided in Section 3.2 below.

3.2 Flux Integration Scheme

The description of the first collision model is hereby supplemented with an outline of the expressions used in the flux integration and their derivation. The integration scheme for flux arriving at point X_s on the spacecraft is depicted in Fig. 3-1. Note that only the plane of incidence is shown in Fig. 3-1; at other azimuth angles the geometry is not co-planar, so 3-D geometrical expressions are used to get the coordinates (ψ, ϕ and radial distancete $(y^2 + z^2)^{1/2}$) from $\vec{\Omega}$ and S ; the derivation of these geometrical relations is straightforward, so that we omit these details in the present report. The total number flux $Q_i(X_s)$ of i exhaust molecules arriving at point X_s is given by the following expression :

$$\begin{aligned}
Q_i(X_s) &= \int d^3\vec{\Omega} \cos\alpha_s \sum_k \int_0^\infty dS \sigma_{ik} h_i N(S) h_k N_A |\vec{U}(S) - \vec{U}_A| \exp[-\eta_k(S)] P_{ik}(S, -\vec{\Omega}) \exp[-\eta_{ik}(S)] \\
\eta_k(S) &= \sum_j \int_0^{t(s)} dt' \sigma_{ik} h_i N(t') |\vec{U}(t') - \vec{U}_A| / |\vec{U}_A| \\
\eta_{ik}(S) &= \sum_j \int_0^S dS' \sigma_{ij} h_j N(S') |\vec{U}_{ik}(S) - \vec{U}(S')| / |\vec{U}_{ik}(S)| \\
()_i \quad ()_j &- \text{ Exhaust species} \quad ()_k - \text{ Ambient species}
\end{aligned} \tag{3-1}$$

These expressions are interpreted as follows. The collision depicted in Fig. 3-1 is between exhaust molecule m_i and ambient molecule m_k . The exhaust molar fractions h_i and ambient molar fractions h_k are assumed uniformly constant, and so are the ambient velocity \vec{U}_A and number density N_A . The exhaust velocity $\vec{U}(S)$ and number density $N(S)$ are function of the location in the flow field defined by $\vec{\Omega}$ and S . These flow variables are computed by first evaluating the coordinates of point $\vec{\Omega}, S$ (Fig. 3-1) in the ring-symmetric CRW from the 3-D geometry, and then employing the power-law approximation outlined in Ch. 2 above, to get all flow variables for a ring-symmetric CRW. In this computation we exploit the fact that characteristic lines fanning out from the nozzle lip are nearly straight lines at the low pressure side of the ring-symmetric CRW.

The $\vec{\Omega}$ integration is performed numerically according to the scheme outlined in Section 3.1 above, as a summation over elements of solid angle ($\Delta^3\vec{\Omega}$) subtended by area elements on the limiting characteristic cone ($\psi = \psi_f$).

The S integration is considerably more complex. The integrand for this integration is derived as follows. Denote by L the line-of-sight distance between point X_s and fan point $\vec{\Omega}, S$. A volume element at the fan point is given by $\Delta v = L^2 \Delta S \Delta^3\vec{\Omega}$. The number of ik pair collisions in Δv per unit time is $\sigma_{ik} h_i N(S) h_k N_A |\vec{U}(S) - \vec{U}_A| \exp[-\eta_k(S)] \Delta v$, where $\eta_k(S)$ denotes the expected number of collisions of ambient molecule k with any exhaust molecule, between its point of entry into the plume and point $\vec{\Omega}, S$. We now multiply this term by $\exp[-\eta_{ik}(S)]$ which is the probability that exhaust molecule i scattered by ambient molecule k would travel from point $\vec{\Omega}, S$ to point X_s collisionlessly, where $\eta_{ik}(S)$ is the expected number of collisions for this path segment. (Note that in Eq. (3-1) the summation in the expression for $\eta_{ik}(S)$ is over all exhaust species j).

The final step in constructing the integrand for the \mathbf{S} integration involves the post-collision directional distribution function $P_{ik}(\mathbf{S}, -\vec{\Omega})$, whose derivation will be given in the sequel. We multiply the integrand by $P_{ik}(\mathbf{S}, -\vec{\Omega}) \Delta^3 \vec{\Omega}_c$ which is the fraction of i exhaust molecules scattered by k ambient molecules into a solid angle element $\Delta^3 \vec{\Omega}_c$ about the unit vector $-\vec{\Omega}$. Considering the flux arriving at a surface area element ΔA_s around point X_s , the solid angle element subtended by ΔA_s is $\Delta^3 \vec{\Omega}_c = \Delta A_s \cos \alpha_s / L^2$. Eq. (3-1) for $Q_i(X_s)$ now follows upon dividing the resulting expression by ΔA_s , thus referring the arriving flux to a unit area at the point of arrival X_s .

Numerically, the \mathbf{S} integration was performed using the classical Runge-Kutta scheme (fourth order). The integration for $\eta_{ik}(\mathbf{S})$ and $\eta_k(\mathbf{S})$ has to be repeated at each point \mathbf{S} . We found reasonable convergence with 4 points in the $\eta_k(\mathbf{S})$ integration and 6 points in the azimuth integration. The \mathbf{S} integration was terminated when convergence was attained (this is the meaning of the upper limit ∞ in the \mathbf{S} integral in Eq. (3-1)). The summation over new strips on the limiting cone ($\psi = \psi_f$) was also terminated upon convergence. The CPU time consumed per target point was about 100 (sec) on IBM 3033 mainframe.

We now take up the derivation of an expression for the post-collision directional distribution function $P_{ik}(\mathbf{S}, -\vec{\Omega})$, which we denote hereafter as $P(-\vec{\Omega})$. We adopt the pair-collision notation presented in Fig. 3-2 for the hard-sphere collision analysis.

As a consequence of conservation of momentum and energy (elastic collisions), the center-of-mass velocity \vec{C}_m and the magnitude of the relative velocity \vec{C}_r are unchanged by the collision [8]. The post-collision velocities are given by :

$$\begin{aligned}\vec{C}_1^* &= \vec{C}_m + \mu_2 \vec{C}_r^* & \vec{C}_2^* &= \vec{C}_m - \mu_1 \vec{C}_r^* \\ \vec{C}_r &= \vec{C}_1 - \vec{C}_2 & \vec{C}_r^* &= \vec{C}_1^* - \vec{C}_2^* \\ \mu_1 &= m_1/(m_1 + m_2) & \mu_2 &= m_2/(m_1 + m_2) \\ \vec{C}_m &= \mu_1 \vec{C}_1 + \mu_2 \vec{C}_2 & |\vec{C}_r^*| &= |\vec{C}_r|\end{aligned}\tag{3-2}$$

The only free parameter in the expressions for post-collision velocities is the orientation of the post-collision relative velocity \vec{C}_r^* . This orientation is uniformly likely to be in any direction in space when hard-spheres collision is assumed [8], as represented by the spherical scattering envelope in

Fig. 3-3. The probability of obtaining \vec{C}_1^* in solid angle element $\Delta^3\vec{\Omega}$ about $-\vec{\Omega}$ (Fig. 3-3) is given by :

$$P(-\vec{\Omega}) = (1/4\pi|\mu_2 \vec{C}_r|^2) (\Delta A / \Delta^3\vec{\Omega}) = (1/4\pi|\cos\delta|) (|\vec{C}_1^*|^2 / |\mu_2 \vec{C}_r|^2) \quad (3-3)$$

where ΔA is an area element on the scattering envelope, whose projection on a plane normal to $\vec{\Omega}$ is $\Delta A |\cos\delta|$. We note that the origin of \vec{C}_m in Fig. 3-3 is external to the scattering envelope, resulting in two possible scattering elements on the sphere. In all the cases that we computed, however (see Ch. 4 below), that point was found to be always internal, so that there was only a single scattering solution with post-collision velocity $\vec{U}_{ik}(S)$ pointing at the spacecraft for any ik pair collision.

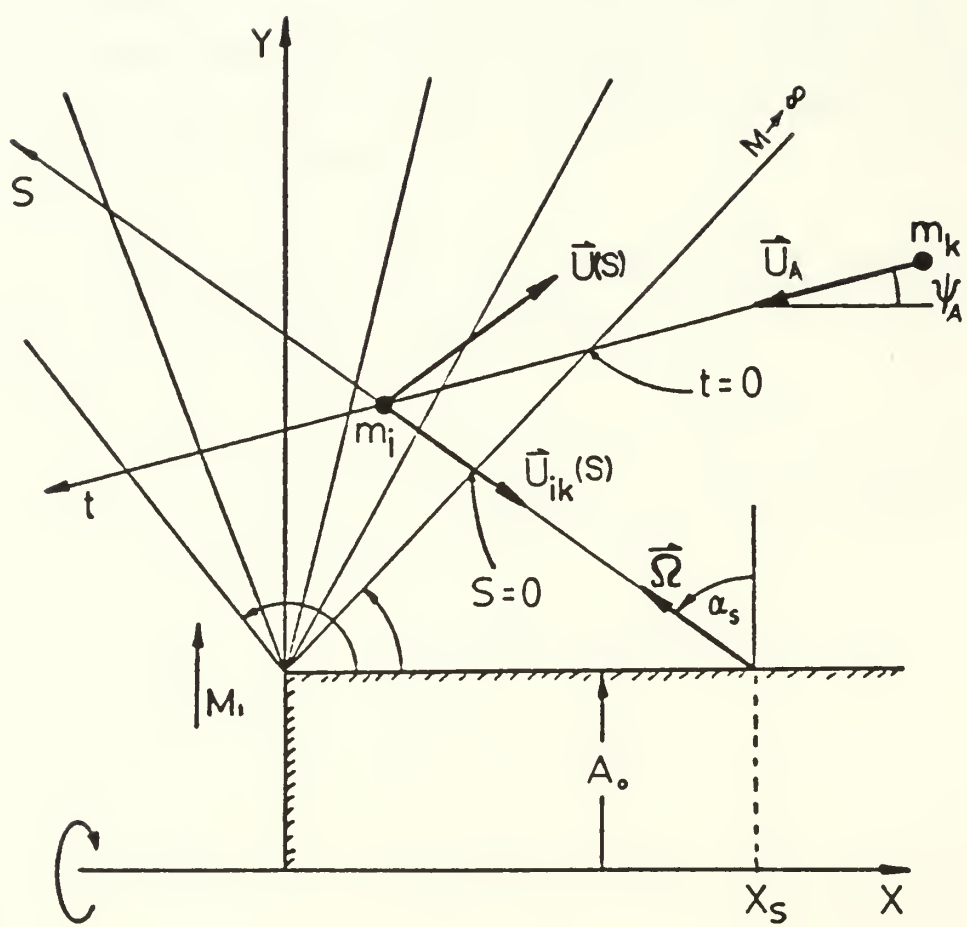


Figure 3-1. Incidence-Plane Description of Flux Integration Scheme.

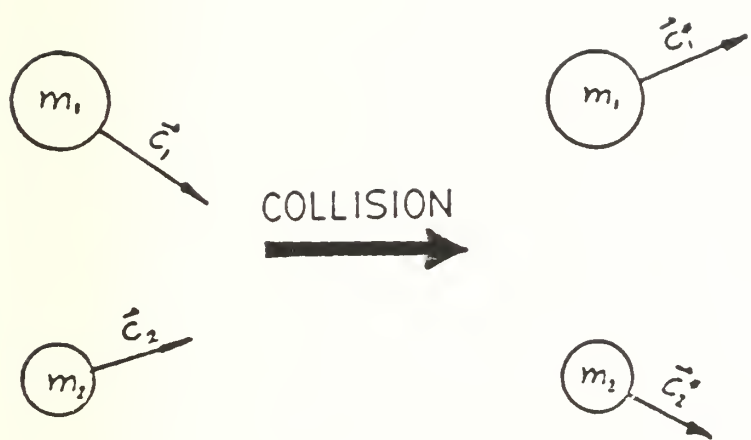


Figure 3-2. Hard-Spheres Collision Notation.

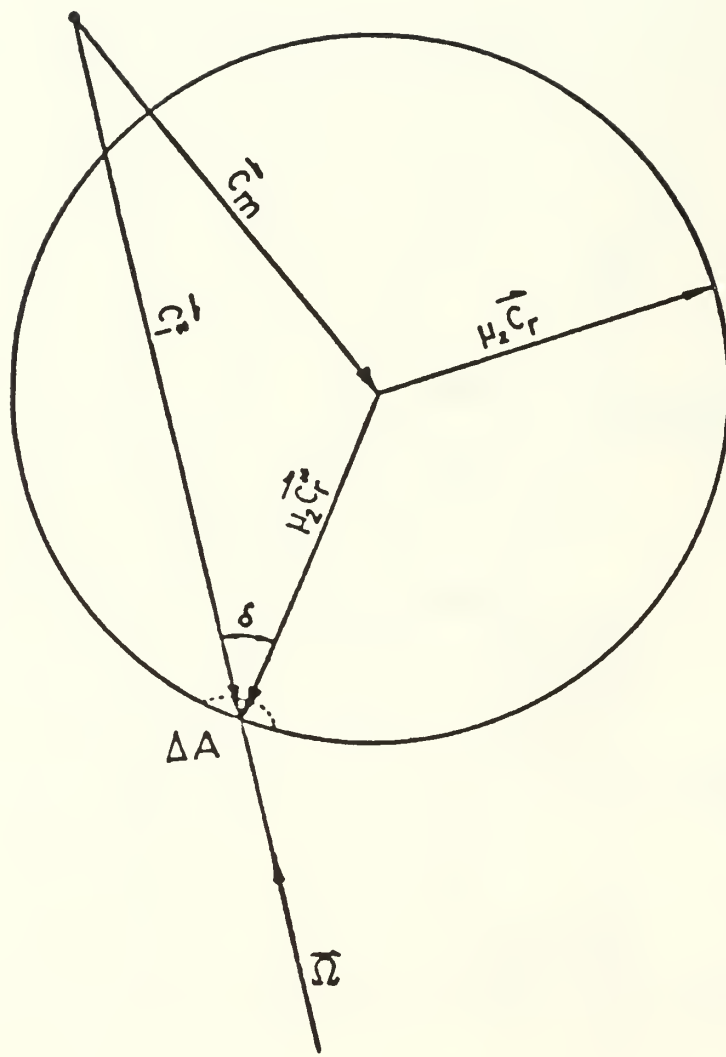


Figure 3-3. Scattering Envelope for Hard-Spheres Collision.

4. RESULTS AND DISCUSSION

We performed several computations of return flux generated by ambient scattering, aimed at demonstrating the expected flux level and its variation with spacecraft target point and orbital attitude angles. In all these computations we assumed that the exhaust flow is as in the typical HF/DF laser case (Table 4-1 below), and that the ambient density and velocity are $N_A = 1 \times 10^{16}$ (molecules/m³) and $U_A = 8$ (km/sec). As an approximation we further assumed that the sole ambient species is molecular nitrogen (molecular weight $W_A = 28$) and that all binary collision cross-sections are uniformly given by $\sigma = \pi D^2$, where D is the molecular diameter (Table 4-1). In each computation we evaluated the combined HF+DF flux by assuming that the molar fraction of DF is zero and the molar fraction of HF is the combined value for both species (Table 4-1) : .091 + .135 = .226. This is justified by the relatively small difference in molecular weight (just 5%) between these two species.

Three sets of flux computation were performed as follows :

- (a) Incidence-plane ($\phi_A = 0$) target points at various distances from the nozzle lip ($X_s = .1$ to $X_s = 10$ (m)), and at constant incidence angle ($\psi_A = 20^\circ$). The results are shown in Fig. 4-1. We observe that the flux is fairly insensitive to X_s . Also shown in Fig. 4-1 are flux computations where the ring-symmetric CRW flow is approximated as a planar CRW (Prandtl-Meyer flow), rather than the power-law as in Eq. (2-1) above. The planar case exhibits a somewhat higher flux, particularly at large X_s .
- (b) Incidence-plane ($\phi_A = 0$) target points at $X_s = 1$ (m) and at various incidence angles ($\psi_A = 0$ to $\psi_A = 40^\circ$). A polar representation of the results is given in Fig. 4-2. Note the sharp decrease in flux as the incidence angle ψ_A approaches the plume limiting angle $\psi_f = 41^\circ$.
- (c) Azimuth angle variation ($\phi_A = 0$ to $\phi_A = 180^\circ$) at a constant location ($X_s = 1$ (m)) and at a constant angle of incidence ($\psi_A = 20^\circ$). A polar representation of the results is given in Fig. 4-3. Observe that flux becomes sensitive to azimuth angle ϕ_A only past $\phi_A = 90^\circ$, where shadowing by the cylindrical spacecraft becomes increasingly dominant.

In addition to return flux we also computed the rms velocity of the arriving molecules. For the target points in group (a), the rms velocity varied between 6000 and 6600 (m/sec) (the higher velocity at smaller X_s), which corresponds to a kinetic energy of about 4 (ev) per molecule (HF).

The maximum return flux arriving at the spacecraft is about 0.15×10^{19} (molecules/m²sec), which corresponds to a surface deposition rate of about 300 monolayers (HF + DF) per hour. This level of contaminating flux may seem to be not outright negligible; however, since return flux is proportional to ambient density, it will be scaled down considerably at higher altitudes (and lower ambient densities).

We observe that the maximum return flux constitutes a fraction of about 2% of the incident ambient flux. This return flux ratio is roughly maintained at almost all target points and attitude angles in groups (a), (b) and (c). The only exceptions are incidence angles near the limiting cone ($\psi = \psi_f$) or at azimuth angles $\varphi_A > 125^\circ$ where shadowing becomes dominant. This observation is interpreted as follows.

Consider the total solid angle subtended by the limiting cone (considered to be infinitely extended in the axial direction) as viewed from a target point (for all lines-of-sight $\vec{\Omega}$ pointing outward of the cylindrical spacecraft surface). It is independent of target location due to the "self-similar" geometry. During each flux computation, we also evaluated the total solid angle subtended by that segment of the cone over which the flux integration was actually performed (see Section 3.2). It was found out that for all but the "shadowed" cases ($\varphi_A > 125^\circ$), this solid angle constituted a fraction of $86 \pm 1\%$ of the solid angle subtended by the infinite cone. We interpret this result as a hint that geometrical "view factors" arising in the course of the flux integration, are not the dominant factor in determining the 2% level of flux ratio. What then are the dominant factors?

For a possible explanation we turn to the flux integration scheme presented in Section 3.2. The flux ratio is obtained upon dividing the integrand in Eq. (3-1) by $N_A U_A$ and setting $h_k = 1$ (since we assume a single species air). The major factors in the flux ratio integrand appear to be the no-collision probabilities $\exp[-\eta_{ik}(S)]$ and $\exp[-\eta_k(S)]$, and the post-collision directional distribution function $P_{ik}(S, -\vec{\Omega})$. The flux-averaged values of these functions in the group (a) computations were found to be as follows : $P_{ik}(S, -\vec{\Omega}) = .09$ to $.10$, $\eta_{ik}(S) = .42$ to $.54$ and $\eta_k(S) = .35$ to $.47$. The flux-averaged Mach number for group (a) points exhibited a much larger variation : between 30 and 80, with the higher Mach numbers obtained at further target points.

These results are interpreted as follows. The ambient no-collision probability $\exp[-\eta_k(S)]$ is sufficiently close to unity, so that in an order-of-magnitude analysis such as the present one, we may disregard this factor. If the velocity ratio in the $\eta_{ik}(S)$ integral of Eq. (3-1) is assumed to be unity (its average value for group (a) points is about 1.4), then the differential in the flux S integration becomes

$\sigma N(S)dS = d\eta_{ik}(S)$. This implies that the flux S integration results in some average value of the only remaining factor : $h_i P_{ik}(S, -\vec{\Omega})$. Since the $\vec{\Omega}$ integration introduces a factor of order unity, the order-of-magnitude estimate for the arriving-to-incident flux ratio is $[h_i P_{ik}(S, -\vec{\Omega})]_{av}$. The value of this estimate is $[h_i P_{ik}(S, -\vec{\Omega})]_{av} = .226 \times .09 \approx .02$, which is about equal to the actual flux ratio for target points in group (a).

When an exhaust flow and orbital parameters (velocity and attitude) are specified, $P_{ik}(S, -\vec{\Omega})$ depends on the choice of molecular collision model (we chose hard spheres), while h_i is uniformly constant. The foregoing reasoning thus establishes the collision model as a significant factor in determining ambient scattering flux levels, to the extent that $P_{ik}(S, -\vec{\Omega})$ is sensitive to the choice of model.

Table 4-1. Typical Operating Conditions of HF/DF Laser Exhaust

Mole fractions	$[H] = .091$	$[HF] = .091$	$[H_2] = .104$	$[DF] = .135$	$[He] = .579$
Average molecular weight		7.14			
Specific heats ratio		1.54			
Stagnation temperature and density		1400 (K)			
		.0075 (kg/m ³)			
Exit Mach number		4.0			
Molecular diameter (hard spheres)		2.5×10^{-10} (m)			
Spacecraft diameter		5.0 (m)			
Nozzle aperture		1.0 (m)			

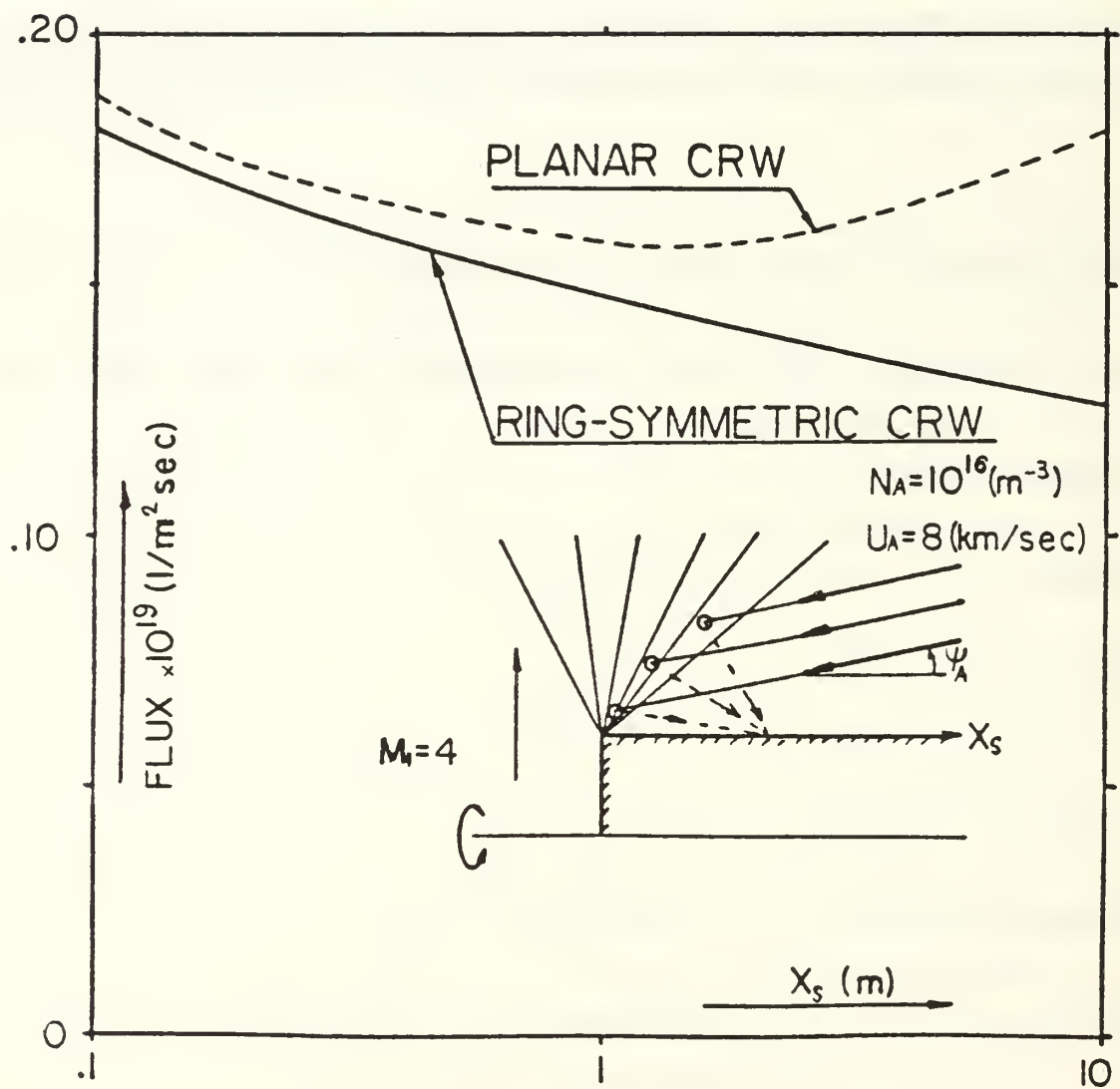


Figure 4-1. Variation of Return Flux with Target Point (X_s). Target Point at Incidence-Plane ($\phi_A = 0$) and Constant Incidence-Angle ($\psi_A = 20^\circ$).

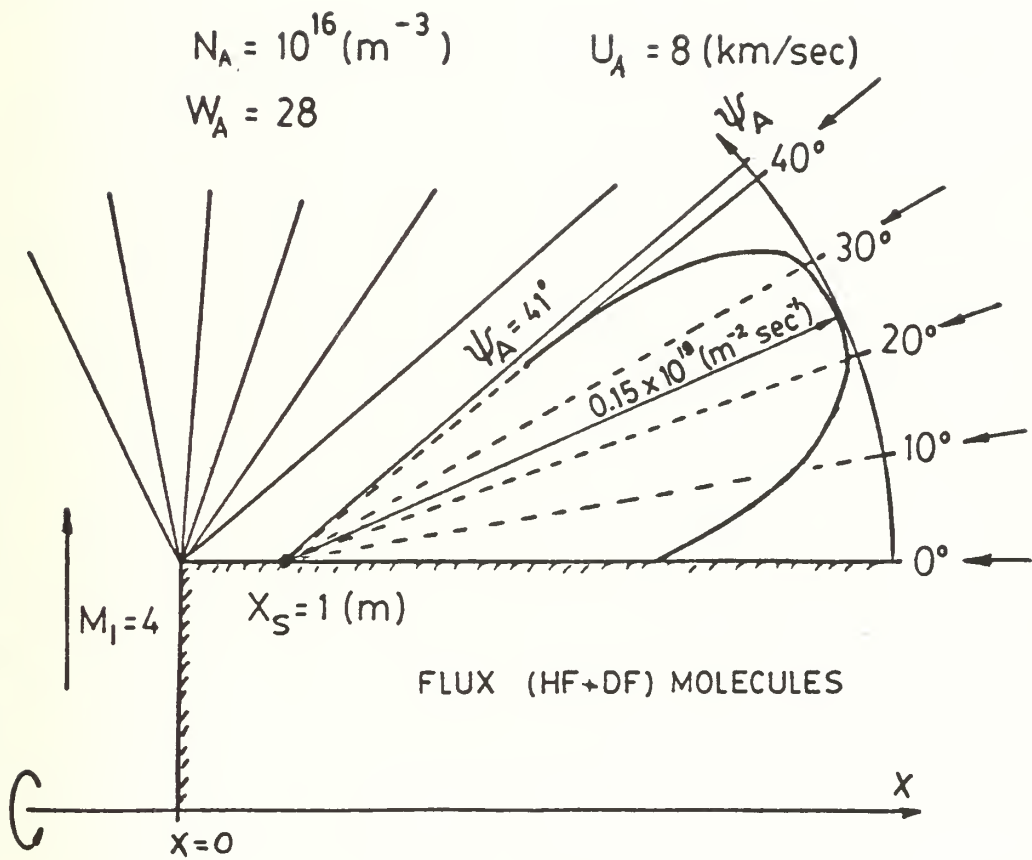


Figure 4-2. Variation of Return Flux with Ambient Incidence Angle (ψ_A). Fixed Target Point ($X_s = 1$ m) Located at Incidence-Plane ($\phi_A = 0$).

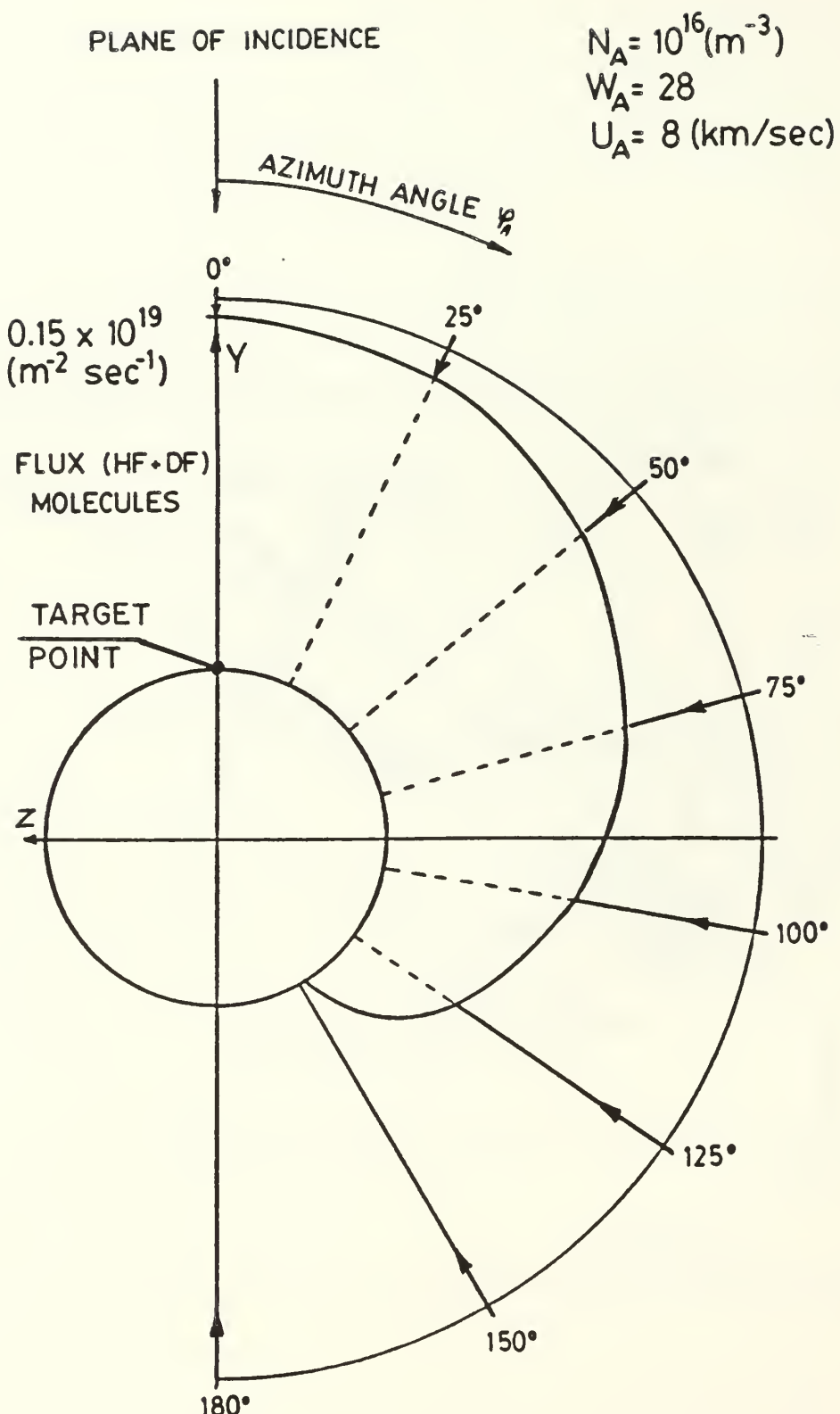


Figure 4-3. Variation of Return Flux with Ambient Azimuth Angle (ϕ_A). Fixed Target Point ($X_s = 1 \text{ m}$) and Ambient Incidence Angle ($\psi_A = 20^\circ$).

5. SPACECRAFT CHARGING

Spacecraft charging is a major concern to spacecraft designers, particularly for missions in GEO and to a lesser extent also in LEO. The exhaust plume of an HF/DF laser operating in the ionosphere (300 to 1000 km altitude) may modify significantly the pre-firing charging pattern of the spacecraft. Two classes of effects may lead to charging modification; they are:

- (a) The exhaust contains large concentrations of HF and DF molecules which are highly electronegative. They may be readily ionized by environmental electrons and change the existing spacecraft charging pattern.
- (b) When the spacecraft is oriented obliquely relative to its orbital velocity and the ambient plasma impinges at the plume boundary, the plume will cast a "shadow" on the downstream side, leading to a very dissimilar charging fluxes on the upstream and downstream halves of the spacecraft.

The knowledge gained in analyzing the ambient scattering effect can be applied to the assessment of the effects of ionospheric plasma on spacecraft charging. We first consider the upstream side of the spacecraft as mentioned in (a) above.

We contend that the exhaust-plasma interaction will not drastically alter the charging pattern of the upstream half. This assessment is established as follows. Consider the fact that ionospheric plasma has a particle number density no higher than 10^{12} (m^{-3}) and energy per particle of at most 1 (ev) (excluding the auroral plasma of polar zones or events of sun storms, where the energy per particle is much higher). Significantly, the Debye length at the highest plasma density is very small : only about 10^{-3} (m); the largest Debye length in the ionosphere is 10^{-1} (m) [9]. Ion thermal velocity is typically lower than orbital velocity, but electron velocity is considerably higher than orbital velocity (at 1 ev the electron velocity is about $U_e = 6 \times 10^5$ m/sec). Hence, ions would typically impinge at the plume as a uniform ion beam with the orbital velocity (like ambient molecules), while electrons are expected to impinge at the plume with their random-oriented thermal velocity.

In view of the results of ambient scattering analysis (Ch. 3 and 4 above), and since ions are subject to similar collision process with exhaust molecules as neutrals, ions will be stopped at the plume fringes much like ambient molecules. By virtue of the small Debye length (typically much smaller than the stopping distance), electrons would not penetrate any further than ions, regardless of their

collision cross-section with exhaust molecules. The familiar plasma sheath that forms at a solid surface, is hence replaced at the plume/plasma boundary by a typically neutral layer whose thickness is of the order of an ion/neutral mean free path, but much larger than the Debye length. Only at the upper altitude range of the ionosphere does the Debye length become comparable to a plume boundary mean free path (about .1 m), but there plasma density and flux are several orders of magnitude lower and charging modification is not likely to be significant at the relatively short firing duration of about 5 minutes.

Elastically scattered ions can be deflected towards the spacecraft as a result of elastic collisions with exhaust molecules, much like neutrals. Referring to our analysis of the return-to-ambient flux ratio (Ch. 4 above), it is clear that the relevant ratio here will be about $1/4\pi$, i.e., of the order of 10% (this is due primarily to the role played by the elastic directional distribution function — see Ch. 4). A change in the plasma-to-surface current of that order is hence possible, but unlikely to affect spacecraft design or operation significantly. The reason is that a design capable of smoothing away the inhomogeneous charge flux at oblique attitudes, will not be sensitive to a change in flux pattern of the order of 10% (in other words, potential differences may be amplified by 10%, which is hardly likely in a sound design to bring about arcing or other threshold phenomena).

Another effect which may potentially be significant in the upstream half is generation of electronegative species (HF^- , DF^-) by plasma electrons impinging at the plume. In the sequel, we examine the magnitude of this effect, concluding that it is negligible.

This estimate is best done by considering \dot{N}^- , which is the rate of production of HF^- and DF^- per unit volume, at a typical point in the exhaust where local Mach number is $M = 30$ (this is typically the lowest average Mach number for the plume region where ambient scattering takes place — see Ch. 4 above). Since energy is released by the electronegative ion formation, the reaction involves a third body as follows :



where M is the third body molecule. We assume a simplified classical kinetic model for this reaction, as follows. The pair HF/M collide with a frequency proportional to the local number density and HF molar fraction, and to the average relative velocity. An electronegative ion formation can occur only if an electron collides with the pair during their collision, which lasts $t_e = D/\bar{C}_r$, where \bar{C}_r is the average relative pair velocity. Based on this classical model, and assuming the same cross-section for

electronegative ion formation as for elastic HF/M collisions, the volume rate of electronegative ion generation is given by :

$$\dot{N}^- = (\pi D^3 N) Nh (\pi D^2 U_e N_e) \quad (5-2)$$

where $(\pi D^3 N)$ is the probability that a certain HF or DF molecule will be in contact (D being molecular hard-sphere diameter) with any other exhaust molecule (whose number density is N). When $(\pi D^3 N)$ is multiplied by hN , where h is the HF + DF molar fraction (Table 4-1), the combined term reads as the number of colliding HF/M pairs per unit volume. Assuming the electronegative formation cross-section is also πD^2 , the factor $\pi D^2 U_e N_e$ where U_e and N_e are electron velocity and number density, renders the expression for electronegative generation rate per unit volume. We note that \bar{C}_r cancels out in deriving Eq. (5-2), so that \dot{N}^- does not depend on temperature. This supports the use of the kinetic approximation in regions of continuum breakdown (plume fringes are such regions).

How is the relative magnitude of \dot{N}^- decided? To do that we multiply \dot{N}^- by $\lambda = 1/\pi D^2 N$, which is the mean free path for a fast moving particle that penetrates the plume. This expression is justified by the fact that most incident particles do collide within a distance of order λ , and when the particles are plasma ions, electrons will adhere to ion spatial distribution by virtue of the small Debye length (smaller than λ). Thus, $\lambda \dot{N}^-$ is the rate of electronegative ion generation per unit area of plume boundary. The ratio β^- between this rate and the incident electron flux is :

$$\beta^- = \lambda \dot{N}^- / N_e U_e = (\pi D^3 N) h = 2.2 \times 10^{-10} \quad (5-3)$$

where $N = 2 \times 10^{19} \text{ (m}^{-3}\text{)}$ which corresponds to Mach number $M = 30$ in the typical case (Table 4-1). The fraction of electron flux captured by HF and DF exhaust molecules to form electronegative ions is so small (due to the pair-formation term $(\pi D^3 N)$), that it cannot appreciably alter the charging flux distribution at the spacecraft surface.

Another possible effect is the recoil of HF^- or DF^- that occurs due to energy released in the electronegative formation reaction. The recoiling species might conceivably reach the surface and contaminate it. The magnitude of the recoil flux is certainly no larger than $\beta^- U_e N_e = 1300 \text{ (m}^{-2} \text{ sec}^{-1}\text{)}$, where we assume the worst case flux : $N_e = 10^{12}$, $U_e = 6 \times 10^5 \text{ (m/sec)}$ which corresponds to about 1 ev energy per electron. This flux level is about 3×10^{-13} monolayers of HF^- and DF^- per hour, so that its contribution to surface contamination is utterly negligible.

The second kind of charging effects (item (b) above) is due to the fact that the exhaust plume is impenetrable to ambient plasma (within a range of sufficiently small distance from the spacecraft, so that no extensive diluting of the plume has taken place). The downstream half of the spacecraft in oblique attitude will be in the "shadow" with respect to incident plasma. As a first approximation we may assume zero plasma flux at the shadowed surface. More accurately, this portion of the spacecraft will be subject to a plasma wake flow. However, it is quite difficult to determine the charging phenomena that take place in such a wake, as indicated by a recent work on solar sails in LEO [9]. Thus, a zero flux at the downstream half seems a practical design assumption.

Can adverse charging effects occur as a result of shadowing the downstream half? This question can be discussed only qualitatively. The reason is that a quantitative analysis requires a lumped-circuit model of the spacecraft external surface [10]. Since such a concrete design is not available, we can only discuss this question qualitatively. Obviously, assuming zero flux to the downstream half during the envisioned 5 minutes of laser firing duration, and requiring that no appreciable voltages between the two halves will evolve, leads to the stipulation that the equivalent-circuit Capacitance \times Resistance should be much smaller than the firing duration.

6. CONCLUDING REMARKS

Our major quantitative conclusion is that for the relatively high ambient density assumed ($N_A = 1 \times 10^{16}$ molecules/m³ which represents Sunspot Maximum at about 200 km) and for the typical HF/DF laser exhaust (Table 4-1), the HF+DF flux backscattered by ambient molecules is several hundred monolayers per hour. This flux level may seem as not outright negligible. However, since ambient scattering flux is proportional to ambient density, it will be scaled down considerably at the lower ambient densities of higher orbital altitudes.

The operational scenario for HF/DF laser envisions 4 or 5 minutes total operating time; hence the contamination by ambient scattering may not be serious due to short operating time.

The effects of laser exhaust plume on spacecraft charging in the ionosphere were examined. It was concluded that the rate of electronegative (HF⁻ and DF⁻) production by impinging electrons was negligible; the low rate is a consequence of the assumption that a third body is required to interact simultaneously with the HF/e or DF/e pair. No significant modification of charging pattern is anticipated. However, at oblique orbital attitudes, the downstream half of the spacecraft will be shadowed from the oncoming ambient plasma. This fact has to be reckoned with in designing a ring-symmetric laser spacecraft.

The emphasis in this work was on the method rather than on results. The first-collision model was demonstrated to be simple to implement in a code. It is considerably simpler than the more general and potentially more accurate Monte Carlo methods commonly used for simulating rarefied flows [8]. We found out that the molecular collision model was all important in determining the return flux level, which is hardly surprising for scattering by single collision. For the same reason, the collision model would also be dominant in a Monte Carlo simulation of the ambient scattering process.

If and when a mathematical accuracy of the first-collision approximation is established for hard-spheres, it might be possible to determine a realistic collision model by comparing computed results with measurements.

This accuracy may be established in either of two ways. One way is by comparison with accurate Monte Carlo computations (using hard-spheres collision model). The other is to seek an estimate of the error incurred by considering just first collisions and ignoring all subsequent ones. This might be achieved by accounting for second collisions in an extended first-collision model, provided a simplified

scheme that will obviate the need for increase in the dimensions of the numerical flux integration can be devised. We are currently considering such second-collision approaches.

7. REFERENCES

- [1] Bird, G. A., "Breakdown of Continuum Flow in Free Jets and Rocket Plumes", Proceedings of 12th Symposium on Rarefied Gas Dynamics. In Volume 74, Progress in Aeronautics and Astronautics, Part II, pp.681, Sam S. Fisher, Editor. Published by AIAA, 1981.
- [2] Falcovitz, J., "Analytic and Numerical Computation of Ring-Symmetric Spacecraft Exhaust Plumes", Report NPS72-86-003CR, Dec. 1986, Naval Postgraduate School, Monterey, CA 93943.
- [3] Liepmann, H. W. and Roshko, A., *Elements of Gasdynamics*, John Wiley, New York, 1957.
- [4] Johnson, F. S., *Satellite Environment Handbook*, Second Edition, Stanford University Press, Stanford, California, 1965.
- [5] Mastrup, F., Broadwell, E., Miller, J. and Jacobs, T. A., "Hydrogen Fluoride Laser Technology Study", Technical Report AFWL-TR-72-28, October 1972.
- [6] Falcovitz, J., "Transient Reactive Exhaust Flow from a Ring-Symmetric HF/DF Space Laser", Report NPS72-87-002CR, Mar. 1987, Naval Postgraduate School, Monterey, CA 93943.
- [7] Falcovitz, J., "Numerical Computation of Ring-Symmetric Spacecraft Exhaust Plumes", Report NPS72-87-001CR, Jan. 1987, Naval Postgraduate School, Monterey, CA 93943.
- [8] Bird, G. A., *Molecular Gas Dynamics*, Clarendon Press, Oxford, 1976.
- [9] Hill, J. R., and Whipple, E. C., "Charging of Large Structures in Space with Application to the Solar Sail Spacecraft (survey)", *Journal of Spacecrafts and Rockets*. Vol. 22, pp. 245-253, 1985.

- [10] Garrett, H. B., "Spacecraft Charging : A Review", pp. 167-226, in *Space Systems and Their Interactions with Earth's Environment*, Henry B. Garrett and Charles P. Pike, editors, Vol. 71 "Progress in Astronautics and Aeronautics", Published by AIAA, 1980.

APPENDIX A. DESCRIPTION OF AMB CODE

A.1 Description of Subroutines

We provide a list of the subroutines in the ambient flux integration code AMB for ring-symmetric cylindrical spacecrafts. Each subroutine is briefly described. Statements are identified by the FORTRAN statement number (columns 1 through 5).

MAIN PROGRAM The 300 loop is intended to enable several (NCASE) reruns with various data in each, all in a single run. Upon calling INIDAT1, parameters depending on data defined in INIDAT are re-computed. The 200 loop is over various XSV(NX) target points. In the 20 loop the flux integration begins : FLUXC is for particle flux and FLXU2C is for the rms of velocity of return flux molecules. All the MAX suffixed parameters denote values at which the integrand had the largest value.

The actual flux integration commences at statement 1 for the summation over strips of constant RF. This summation is terminated when convergence is attained (to within EPSR). The inner loop 2 is over azimuth angle PHI. Note that the target points are generally not in the plane of incidence (PHIA.NE.0), so that no symmetry can be assumed in the PHI integration, and it is performed twice in order to cover the entire range in PHI (IPAR = 1 for PHI.GT.0, IPAR = 2 for PHI.LT.0). The flux integration along the line-of-sight is done by calling FLUX.

INIDAT Initialization of data. There is no input file for this code. INIDAT1 is for parameters computed from the data defined by calling INIDAT.

SOF Stopping routine, called when an error is detected. Here we also trigger a system error by computing DSQRT(-1), in order to obtain a calling sequence printout by the operating system.

FLUX This routine calls SUMT for flux integration of one exhaust species at a time.

LIMIT Here we compute the point of intersection of the line-of-sight with the leading characteristic cone. If they do not intersect, the distance of the intersecting point TLIM is set to a very large number.

- SUMT This is the line-of-sight integration routine. Runge-Kutta scheme is used (even though an explicit integral is computed). Note that ETAK and ETAIK have to be computed through a separate integration at each point of the line-of-sight integration. The integration step DT ($T = S/RF$) is re-adjusted at each integration step. The integration is terminated when convergence is attained (to within EPST).
- FETA Here the integrand for the line-of-sight flux integration is evaluated. The hard-spheres collision model is used to determine the post-collision directional distribution factor PIK. The flux-average of any variable (such as UIK**2 in present version), can be computed by summing it multiplied by flux and subsequently dividing by the total arriving flux (see loop 31 in MAIN PROGRAM).
- PATHIK Here the molecular thickness ETAIK of the I exhaust species scattered by the K ambient molecule, is computed by integration along the line-of-sight.
- FT This routine computes the integrand for the ETAIK integration in PATHIK.
- PATHK The analog to PATHIK for K ambient molecule. TAU is the normalized integration variable along the trajectory of the penetrating ambient molecule. Note that SHADOW=.TRUE. when the trajectory passes through the cylindrical spacecraft surface before entering the fan.
- FTAU Computes the integrand for the ETAK integration in PATHK.
- FAN Computes the fan coordinates PSI, XP, YP for a point on the line-of-sight. It is used to determine the Mach number and flow angle from the power-law approximation (see MATCH).
- FANT Computes the fan coordinates PSI, XP, YP for a point on the ambient molecule trajectory.
- HMSET Prepares the vector HMV(I) which is the value of the H(M) integral at a set of Mach number values (equally spaced in inverse Mach number). This vector is used to compute H(M) for an arbitrary M (see HINTER), since this function is needed in the power-law approximation of flow in a ring-symmetric fan. Subsequent routines MFUNC, HINTER, MATCH and AREAF are all used to implement this approximation.

MFUNC Computes the integrand for the H(M) integration in HMSET.

HINTER Computes H(M) for a given M, from HMV(I) by linear interpolation. Note that the interpolation is done with inverse Mach number as the independent variable.

MATCH Here the approximation to the "inverse problem" of finding the Mach number at a single point in the ring-fan is implemented. An iteration scheme is used to determine the fan characteristic passing through the given point [2] .

AREAF Mach number is computed from value of area ratio function. Newton-Raphson iterations are used.

A.2 Listing of AMB code

```

C$OPTIONS LIST                                AMB0001
C  AMBIENT. SCATTERING FROM A RING PLUME BY AMBIENT AIR.      AMB0002
  IMPLICIT REAL*8(A-H,O-Z)                                AMB0003
  COMMON /GAMA/G,G1,G2,G3,G4,G5,G6,G7,G8,G9,G10,G11,G12,G13,G14,G15,AMB0004
  1          G16,G17,G18,G19,G20                                AMB0005
  COMMON /PAR/C0,ENO,EM1,D,SIGMA,TLIM,DR0,EL0,Q0,T0,FACT,ALOGF,AMB0006
  1          DPSI0,DTMAX,DETA0,ETALIM,XSI,XSF                AMB0007
  COMMON /NPAR/NPHI,IPAR,NP,NR,NX,NXS,NS,NSPEC,NS1,NS2,NTAU0,NETAO,AMB0008
  1          NAMB,NCASE,ICASE,IFAN                            AMB0009
  COMMON /GEOM/APF,PAI,PAI2,W,SW,CW,BETA,CBETA,PSI1,SPSI1,AMB0010
  1          CPSI1,PSIF,SPSIF,CPSIF,AK,SK,CK,A0,RF,XF,YF,ZF,AMB0011
  2          PHISOF,PHIF,SPHIF,CPHIF,DYMIN,RMIN,XS,DIST,X0,Y0,Z0,AMB0012
  3          DY0,DEG,PSIN,ST1,CT1,OMEGX,OMEGY,OMEGZ,XSV(21)    AMB0013
  COMMON /EPSIL/EPSETA,EPST,EPSR                  AMB0014
  COMMON /EXTREM/TEXT(5),ETAEXT(5),ETAKXT(5),PHIEXT(5),AMB0015
  1          PSIEXT(5),EMEXT(5),FEXT(5),WEXT(5),              AMB0016
  2          TMAX(5),ETAKMX(5),ETAMAX(5),PSIMAX(5),          AMB0017
  3          EMMAX(5),FMAX(5),                            AMB0018
  4          RFMAX(5),PHIFMX(5),PHIMAX(5),WMAX(5)           AMB0019
  COMMON /COUNTS/ICONTIC,ICONTT,ICNTOT,ICNTMX,IQTOT(5),ISHAD(5) AMB0020
  COMMON /SPEC/WAV,XC(5),WC(5),WR(5),XNAME(5),QFC(5),QDC(5),AMB0021
  1          QU2C(5),FLUXC(5),OMEGA(5),FLXU2C(5),URMSC(5)   AMB0022
  COMMON /AMBIEN/ENA,UA,PSIA,PHIA,HA(3),WA(3),              AMB0023
  1          UAX,UAY,UAZ,AA,BA,CA,RA,XA,YA,ZA,SHADOW        AMB0024
  COMMON /POINT/XP,YP,XCOR,YCOR                   AMB0025
  LOGICAL SHADOW                                 AMB0026
  DIMENSION DSUMF(5),DSUMD(5),DSUMAX(5),DSUMU2(5)       AMB0027
  NCASE=1                                         AMB0028
  DO 300 ICASE=1,NCASE                           AMB0029
  CALL INIDAT                                     AMB0030
  GO TO (301,302,303,304,305,306,307,308,309,310,AMB0031
  1          311,312,313,314,315,316,317,318,319,320),ICASE AMB0032
301  CONTINUE                                     AMB0033
  IFAN=1                                         AMB0034
  NXS=3                                           AMB0035
  XSI=0.1D0                                      AMB0036
  GO TO 399                                       AMB0037
302  CONTINUE                                     AMB0038
  PHIA=20.D0/DEG                                 AMB0039
  GO TO 399                                       AMB0040
303  CONTINUE                                     AMB0041
  PHIA=50.D0/DEG                                 AMB0042
  GO TO 399                                       AMB0043
304  CONTINUE                                     AMB0044
  PHIA=75.D0/DEG                                 AMB0045
  GO TO 399                                       AMB0046
305  CONTINUE                                     AMB0047
  PHIA=100.D0/DEG                                AMB0048
  GO TO 399                                       AMB0049
306  CONTINUE                                     AMB0050
  PHIA=125.D0/DEG                                AMB0051
  GO TO 399                                       AMB0052
307  CONTINUE                                     AMB0053
  PHIA=150.D0/DEG                                AMB0054
  GO TO 399                                       AMB0055
308  CONTINUE                                     AMB0056
  PHIA=175.D0/DEG                                AMB0057
  GO TO 399                                       AMB0058
309  CONTINUE                                     AMB0059
  GO TO 399                                       AMB0060
310  CONTINUE                                     AMB0061
  GO TO 399                                       AMB0062
311  CONTINUE                                     AMB0063
  GO TO 399                                       AMB0064
312  CONTINUE                                     AMB0065
  GO TO 399                                       AMB0066
313  CONTINUE                                     AMB0067
  GO TO 399                                       AMB0068
314  CONTINUE                                     AMB0069
  GO TO 399                                       AMB0070
315  CONTINUE                                     AMB0071
  GO TO 399                                       AMB0072

```

```

316  CONTINUE AMB0073
      GO TO 399 AMB0074
317  CONTINUE AMB0075
      GO TO 399 AMB0076
318  CONTINUE AMB0077
      GO TO 399 AMB0078
319  CONTINUE AMB0079
      GO TO 399 AMB0080
320  CONTINUE AMB0081
      GO TO 399 AMB0082
399  CONTINUE AMB0083
      PRINT 101 AMB0084
101  FORMAT('1') AMB0085
C     CALL INDAT1 AMB0086
C
C     DO 200 NX=1,NXS AMB0087
C     XS=XSV(NX) AMB0088
C (X0,Y0,Z0) IS THE POINT AT WHICH FLUX AND DENSITY ARE COMPUTED. AMB0089
C THE NORMAL TO THE SURFACE AT (X0,Y0,Z0) IS PARALLEL TO Y-AXIS. AMB0090
C
C     X0=XS AMB0091
C     Y0=A0 AMB0092
C     Z0=0. AMB0093
C
C     DO 20 NS=NS1,NS2 AMB0094
C     FLUXC(NS)=0. AMB0095
C     FLXU2C(NS)=0. AMB0096
C     OMEGA(NS)=0. AMB0097
C     DSUMAX(NS)=0. AMB0098
C     IQTOT(NS)=0. AMB0099
C     ISHAD(NS)=0. AMB0100
C     TMAX(NS)=-1.D 44 AMB0101
C     ETAKMX(NS)=-1.D 44 AMB0102
C     PHIMAX(NS)=-1.D 44 AMB0103
C     PHIFMX(NS)=-1.D 44 AMB0104
C     WMAX(NS)=-1.D 44 AMB0105
C     PSIMAX(NS)=-1.D 44 AMB0106
C     ETAMAX(NS)=-1.D 44 AMB0107
C     RFMAX(NS)=-1.D 44 AMB0108
C     EMMAX(NS)=-1.D 44 AMB0109
C     FMAX(NS)=-1.D 44 AMB0110
C
20   CONTINUE AMB0111
RN=RMIN AMB0112
APF=A0-0.5D0*DRO*SPSIF AMB0113
NR=0 AMB0114
1    NR=NR+1 AMB0115
DR=DRO AMB0116
DR=DRO*(APF/A0) AMB0117
C     DR=DRO*(1.D0+0.4D0*DRO/XS)**NR AMB0118
RF=RN+DR/2.D0 AMB0119
APF=A0+RF*SPSIF AMB0120
PHISOF=DACOS(A0/APF) AMB0121
C     DPHI0=0.1D0 AMB0122
C     NPHI=PHISOF/DPHI0+2 AMB0123
DPHI=PHISOF/DBLE(NPHI) AMB0124
DO 21 NS=NS1,NS2 AMB0125
DSUMF(NS)=0. AMB0126
DSUMU2(NS)=0. AMB0127
DSUMD(NS)=0. AMB0128
21   CONTINUE AMB0129
DOMEGR=0. AMB0130
DO 2 NP=1,NPHI AMB0131
DO 2 IPAR=1,2 AMB0132
PHIF=(DBLE(NP)-0.5D0)*DPHI AMB0133
IF(IPAR.EQ.2) PHIF=-PHIF AMB0134
C     CALL FLUX AMB0135
C
C     CROSS1=OMEGY AMB0136
C     CROSS2=(SPSIF)*(-OMEGX)+(-CPSIF*CPHIF)*(-OMEGY)+ AMB0137
1     (-CPSIF*SPHIF)*(-OMEGZ) AMB0138
IF(CROSS1.LE.0.) AMB0139
1CALL SOF('DIRECTION COSINE OF SURFACE NORMAL SHOULD BE POSITIVE') AMB0140

```

```

IF(CROSS2.LE.0.) AMB0145
1CALL SOF('NORMAL TO LIMITING CONE HAS NEGATIVE PROJECTION ON LINE-AMB0146
1OF-SIGHT') AMB0147
DOMEGR=DOMEGR+DOMEGA AMB0148
DOMEGA=CROSS2*DPHI*APF*DR/DIST**2 AMB0149
DO 24 NS=NS1,NS2 AMB0150
DSUMF(NS)=DSUMF(NS)+DOMEGA*QFC(NS)*CROSS1 AMB0151
DSUMU2(NS)=DSUMU2(NS)+DOMEGA*QU2C(NS)*CROSS1 AMB0152
IF(DSUMAX(NS).GT.DOMEGR*QFC(NS)*CROSS1) GO TO 24 AMB0153
DSUMAX(NS)=DOMEGA*QFC(NS)*CROSS1 AMB0154
TMAX(NS)=TEXT(NS) AMB0155
ETAKMX(NS)=ETAKXT(NS) AMB0156
PHIMAX(NS)=PHIEXT(NS)*DEG AMB0157
PHIFMX(NS)=PHIF*DEG AMB0158
WMAX(NS)=WEXT(NS)*DEG AMB0159
PSIMAX(NS)=PSIEXT(NS)*DEG AMB0160
ETAMAX(NS)=ETAEXT(NS) AMB0161
RFMAX(NS)=RF AMB0162
EMMAX(NS)=EMEXT(NS) AMB0163
FMAX(NS)=QFC(NS)*XC(NS)*Q0 AMB0164
24 CONTINUE AMB0165
2 CONTINUE AMB0166
DO 26 NS=NS1,NS2 AMB0167
FLUXC(NS)=FLUXC(NS)+DSUMF(NS) AMB0168
FLXU2C(NS)=FLXU2C(NS)+DSUMU2(NS) AMB0169
OMEGA(NS)=OMEGA(NS)+DOMEGR AMB0170
26 CONTINUE AMB0171
RN=RN+DR AMB0172
IF(NR.LE.2) GO TO 1 AMB0173
IF(NR.GT.99) GO TO 10 AMB0174
DO 27 NS=NS1,NS2 AMB0175
IF(FLUXC(NS).EQ.0.) GO TO 27 AMB0176
ERR=(DSUMF(NS)/FLUXC(NS))/DOMEGR AMB0177
IF(ERR.GT.EPSR) GO TO 28 AMB0178
27 CONTINUE AMB0179
GO TO 10 AMB0180
28 CONTINUE AMB0181
GO TO 1 AMB0182
10 CONTINUE AMB0183
DO 31 NS=NS1,NS2 AMB0184
FLUXC(NS)=XC(NS)*FLUXC(NS)*Q0 AMB0185
OMEGA(NS)=OMEGA(NS)/(2.D0*PAI*DCOS(PSIF/2.D0)**2) AMB0186
FLXU2C(NS)=XC(NS)*FLXU2C(NS)*Q0 AMB0187
URMSC(NS)=0. AMB0188
IF(FLUXC(NS).EQ.0.) GO TO 31 AMB0189
URMSC(NS)=DSQRT(FLXU2C(NS)/FLUXC(NS)) AMB0190
C AVERAGE EM (SEE FETA) AMB0191
URMSC(NS)= FLXU2C(NS)/FLUXC(NS) AMB0192
31 CONTINUE AMB0193
PRINT 11,NX,NR,XS,RF,DR,PHISOF*DEG AMB0194
11 FORMAT(//1X,'NX,NR,XS,RF,DR,PHISOF=',2I4,3D13.4,F8.4, AMB0195
1 3X,'FLUX AND EXTREMA VALUES, ALL SPECIES:/*) AMB0196
PRINT 12 AMB0197
12 FORMAT(/1X,' NAME ',' IQTOT',' ISHAD', AMB0198
1 ' FMAX ',' OMEGA',' TMAX', AMB0199
2 ' ETAKMX',' ETAMAX',' PSIMAX', AMB0200
3 ' EMMAX',' RFMAX',' PI-WMAX', AMB0201
4 ' URMSC',' FLUXC / LOG') AMB0202
DO 14 NS=NS1,NS2 AMB0203
DLF=0. AMB0204
IF(FLUXC(NS).NE.0) AMB0205
1 DLF=DLG10(FLUXC(NS))+100.D0+1.D-11 AMB0206
IDL F=DLF AMB0207
DLF=DLF-DBLE(IDLF) AMB0208
PRINT 13,XNAME(NS),IQTOT(NS),ISHAD(NS),FMAX(NS),OMEGA(NS), AMB0209
1 TMAX(NS),ETAKMX(NS),ETAMAX(NS), AMB0210
2 PSIMAX(NS),EMMAX(NS),RFMAX(NS), AMB0211
3 180.D0-WMAX(NS),URMSC(NS), AMB0212
4 FLUXC(NS),DLF AMB0213
13 FORMAT(1X,A6,2I6,D10.3,4F8.4,4F8.1,F8.2,D10.3,'/',F4.2) AMB0214
14 CONTINUE AMB0215
200 CONTINUE AMB0216

```

```

PRINT 102 AMB0217
102 FORMAT(///1X,'END RING RUN',///) AMB0218
300 CONTINUE AMB0219
STOP AMB0220
END AMB0221
SUBROUTINE INIDAT AMB0222
IMPLICIT REAL*8(A-H,O-Z) AMB0223
REAL*8 LAMDAO,LAMDA1 AMB0224
CHARACTER*8 XNAME,XNAMED AMB0225
COMMON /GAMA/G,G1,G2,G3,G4,G5,G6,G7,G8,G9,G10,G11,G12,G13,G14,G15,AMB0226
1 G16,G17,G18,G19,G20 AMB0227
COMMON /PAR/C0,ENO,EM1,D,SIGMA,TLIM,DR0,EL0,Q0,T0,FACT,ALOGF, AMB0228
1 DPSI0,DTMAX,DETA0,ETALIM,XSI,XSF AMB0229
COMMON /NPAR/NPHI,IPAR,NP,NR,NX,NXS,NS,NSPEC,NS1,NS2,NTAU0,NETAO, AMB0230
1 NAMB,NCASE,ICASE,IFAN AMB0231
COMMON /GEOM/APF,PAI,PAI2,W,SW,CW,BETA,SBETA,CBETA,PSI1,SPSII, AMB0232
1 CPSII,PSIF,SPSIF,CPSIF,TPSIF,AK,SK,CK,A0,RF,XF,YF,ZF,AMB0233
2 PHISOF,PHIF,SPHIF,CPHIF,DYMIN,RMIN,XS,DIST,X0,Y0,Z0, AMB0234
3 DY0,DEG,PSIN,ST1,CT1,OMEGX,OMEGY,OMEGZ,XSV(21) AMB0235
COMMON /EPSIL/EPSETA,EPST,EPSR AMB0236
COMMON /EXTREM/TEXT(5),ETAEXT(5),ETAKXT(5),PHIEXT(5), AMB0237
1 PSIEXT(5),EMEXT(5),FEXT(5),WEXT(5), AMB0238
2 TMAX(5),ETAKMX(5),ETAMAX(5),PSIMAX(5), AMB0239
3 EMMAX(5),FMAX(5), AMB0240
4 RFMAX(5),PHIFMX(5),PHIMAX(5),WMAX(5) AMB0241
COMMON /COUNTS/ICONTC,ICONTT,ICNTOT,ICNTMX,IQTOT(5),ISHAD(5) AMB0242
COMMON /SPEC/WAV,XC(5),WC(5),WRC(5),XNAME(5),QFC(5),QDC(5), AMB0243
1 QU2C(5),FLUXC(5),OMEGA(5),FLXU2C(5),URMSC(5) AMB0244
COMMON /AMBIEN/ENA,UA,PSIA,PHIA,HA(3),WA(3), AMB0245
1 UAX,UAY,UAZ,AA,BA,CA,RA,XA,YA,ZA,SHADOW AMB0246
COMMON /POINT/XP,YP,XCOR,YCOR AMB0247
LOGICAL SHADOW AMB0248
DIMENSION XCD(5),WCD(5),XNAMED(5) AMB0249
DATA XCD/.091D0,.091D0,.104D0,.135D0,.579D0/ AMB0250
DATA WCD/1.00D0,20.0D0,2.00D0,21.0D0,4.00D0/ AMB0251
DATA XNAMED/' H ',' HF ',' H2 ',' DF ',' HE '/ AMB0252
DATA IFIRST/0/ AMB0253
IFAN=2 AMB0254
PAI=4.D0*Datan(1.D0) AMB0255
PAI2=PAI/2.D0 AMB0256
DEG=180.D0/PAI AMB0257
AR=8.3143D3 AMB0258
AV=6.022D 26 AMB0259
C OMEGAC=0.5 IS FOR HARD SPHERE COLLISIONS, AMB0260
C AN AVERAGE RECOMMENDED VALUE IS ABOUT OMEGAC=0.75 AMB0261
OMEGAC=0.5D0 AMB0262
NSPEC=5 AMB0263
NS1=2 AMB0264
NS2=2 AMB0265
DO 51 NS=1,NSPEC AMB0266
XC(NS)=XCD(NS) AMB0267
WC(NS)=WCD(NS) AMB0268
XNAME(NS)=XNAMED(NS) AMB0269
51 CONTINUE AMB0270
C COMBINE HF AND DF MOLE FRACTIONS INTO HF FRACTION AMB0271
XC(2)=XC(2)+XC(4) AMB0272
XC(4)=0. AMB0273
C
A0=2.5D0 AMB0274
EM1=4.D0 AMB0275
RH00=0.0075D0 AMB0276
T0=1400.D0 AMB0277
G=1.54D0 AMB0278
D=2.5D-10 AMB0279
NXS=1 AMB0280
XSI=1.0D0 AMB0281
XSF=10.D0 AMB0282
C AMBIENT AIR AMB0283
ENA=1.00D 16 AMB0284
UA=8.D 3 AMB0285
NAMB=3 AMB0286
WA(1)=28.D0 AMB0287
AMB0288

```

```

WA(2)=32.D0 AMB0289
WA(3)=16.D0 AMB0290
HA(1)=1.D0 AMB0291
HA(2)=0. AMB0292
HA(3)=0. AMB0293
PSIA=20.D0/DEG AMB0294
PHIA=0.00D0/DEG AMB0295
C INTEGRATION PARAMETERS AMB0296
NPHI=6 AMB0297
NTAU0=4 AMB0298
NETA0=4 AMB0299
ICNTMX=100 AMB0300
RMIN=0. AMB0301
DR0=0.10D0 AMB0302
DPSI0=0.20D0 AMB0303
DTMAX=1.0D0 AMB0304
DETA0=0.50D0 AMB0305
ETALIM=10.D0 AMB0306
EPST=0.5D0 AMB0307
EPSR=0.3D0 AMB0308
FACT=1.D 20 AMB0309
RETURN AMB0310
*****
C COMPUTATION OF DATA-DEPENDENT PARAMETERS AMB0311
***** AMB0312
ENTRY INDAT1 AMB0313
***** AMB0314
C AL0GF=DLOG(FACT) AMB0315
WAV=0. AMB0316
DO 52 NS=1,NSPEC AMB0317
WAV=WAV+XC(NS)*WC(NS) AMB0318
52 CONTINUE AMB0319
DO 53 NS=1,NSPEC AMB0320
WRC(NS)=WC(NS)/WAV AMB0321
53 CONTINUE AMB0322
SIGMA=PAI*D**2 AMB0323
EN0=RHO0*AV/WAV AMB0324
C0=DSQRT(G*AR*T0/WAV) AMB0325
XSV(1)=XSI AMB0326
IF(NXS.EQ.1) GO TO 12 AMB0327
DXL=(DLOG(XSF)-DLOG(XSI))/(DBLE(NXS)-1.D0) AMB0328
XLI=DLOG(XSI) AMB0329
DO 11 NX=2,NXS AMB0330
XSV(NX)=DEXP(XLI+(DBLE(NX)-1.D0)*DXL) AMB0331
11 CONTINUE AMB0332
12 CONTINUE AMB0333
G1=(G-1.D0)/2.D0 AMB0334
G2=(G+1.D0)/(2.D0*(G-1.D0)) AMB0335
G3=G/2.D0 AMB0336
G4=(G+1.D0)/(G-1.D0) AMB0337
G5=DSQRT((G+1.D0)/(G-1.D0)) AMB0338
G6=1.D0/(G-1.D0) AMB0339
G7=2.D0/(G+1.D0) AMB0340
G8=(0.5D0*(G+1.D0)**2/(G-1.D0))**(1.D0/(G+1.D0))* AMB0341
1 ((G+1.D0)/(G-1.D0))**(G-1.D0)/(G+1.D0)) AMB0342
G9=(G+3.D0)/(2.D0*(G-1.D0)) AMB0343
G10=(7.D0-3.D0*G)/(2.D0*(G-1.D0)) AMB0344
G11=(5.D0-3.D0*G)/(2.D0*(G-1.D0)) AMB0345
G13=(2.D0-G)/(2.D0*(G-1.D0)) AMB0346
G14=G/(2.D0*(G-1.D0)) AMB0347
G15=(G+1.D0)/(3.D0-G) AMB0348
ZETA1=G5*DATAN(DSQRT(EM1**2-1.D0)/G5) AMB0349
AMU1=DASIN(1.D0/EM1) AMB0350
PSI1=PAI2+AMU1 AMB0351
SPSI1=DSIN(PSI1) AMB0352
CPSI1=DCOS(PSI1) AMB0353
PSIF=PAI2+AMU1+ZETA1-G5*PAI2 AMB0354
SPSIF=DSIN(PSIF) AMB0355
CPSIF=DCOS(PSIF) AMB0356
TPSIF=DTAN(PSIF) AMB0357
TETA1=PSI1-AMU1 AMB0358
ST1=DSIN(TETA1) AMB0359
ST1=DSIN(TETA1) AMB0360

```

```

CT1=DCOS(TETA1) AMB0361
Q0=ENA*UA AMB0362
LAMDA0=1.D0/(DSQRT(2.D0)*SIGMA*ENO) AMB0363
LAMDA1=LAMDA0*(1.D0+G1*EM1**2)**(G6-OMEGAC+0.5D0) AMB0364
AA=DCOS(PSIA) AMB0365
BA=DSIN(PSIA)*DCOS(PHIA) AMB0366
CA=DSIN(PSIA)*DSIN(PHIA) AMB0367
UAX=-UA*AA AMB0368
UAY=-UA*BA AMB0369
UAZ=-UA*CA AMB0370
XCOR=0. AMB0371
YCOR=A0 AMB0372
C AMB0373
PRINT 201,NSPEC,XNAME AMB0374
201 FORMAT(/1X,'SPECIES DATA NSPEC=',I3/ AMB0375
1 1X,'SPECIES NAMES ',11(2X,A6,2X)) AMB0376
PRINT 202,XC AMB0377
202 FORMAT( 1X,'MOLE FRACTION XC=',11(F8.4,2X)) AMB0378
PRINT 203,WC AMB0379
203 FORMAT( 1X,'MOL. WEIGHT WC=',11(F8.4,2X)) AMB0380
PRINT 21,AR,AV,WAV,G,RHOO,T0,ENO,C0,D AMB0381
21 FORMAT(/1X,'THERMODYNAMIC DATA'/ AMB0382
1 1X,'AR,AV,WAV,GAMMA=',2X,2D14.5,2F9.3/ AMB0383
2 1X,'RHOO,T0,ENO,C0,D=',D12.4,F8.0,D13.5,2D12.4) AMB0384
PRINT 22,EM1,PSI1*DEG,PSIF*DEG, AMB0385
1 A0,LAMDA0,LAMDA1 AMB0386
22 FORMAT(/1X,'FLOW AND GEOMETRY DATA'/ AMB0387
1 1X,'EM1,PSI1,PSIF=',3F9.3/ AMB0388
2 1X,'A0,LAMDA0,LAMDA1=',F9.3,2D13.4) AMB0389
PRINT 23,DPSI0,DTMAX,DETA0,ETALIM,DRO,RMIN, AMB0390
1 EPST,EPSR, AMB0391
2 NPHI,NTAU0,NETAO AMB0392
23 FORMAT(/1X,'INTEGRATION DATA'/ AMB0393
1 1X,'DPSI0,DTMAX,DETA0,ETALIM=',4F9.4/ AMB0394
2 1X,'DRO,RMIN,=',2D13.4/ AMB0395
3 1X,'EPST,EPSR=',2D12.3/ AMB0396
4 1X,'NPHI,NTAU0,NETAO=',3I6) AMB0397
PRINT 24,ENA,UA,PSIA*DEG,PHIA*DEG AMB0398
24 FORMAT(/1X,'ABBREVIATED AIR DATA'/ AMB0399
1 1X,'ENA,UA=',2D13.4/ AMB0400
2 1X,'PSIA,PHIA=',2F9.1) AMB0401
GO TO (251,252), IFAN AMB0402
AMB0403
251 CONTINUE AMB0404
PRINT 2510, IFAN AMB0405
2510 FORMAT(/1X,'RING-FAN APPROXIMATED AS PLANAR. IFAN=',I4) AMB0406
GO TO 250 AMB0407
252 CONTINUE AMB0408
PRINT 2520, IFAN AMB0409
2520 FORMAT(/1X,'RING-FAN APPROXIMATED BY MATCHED APPROXIMATION.', AMB0410
1 4X,'IFAN=',I4) AMB0411
250 CONTINUE AMB0412
PRINT 29 AMB0413
29 FORMAT(///1X,'END DATA'///) AMB0414
IF(IFIRST.EQ.0.AND.IFAN.EQ.2) AMB0415
1CALL HMSET AMB0416
IF(IFAN.EQ.2) IFIRST=IFIRST+1 AMB0417
RETURN AMB0418
END AMB0419
C$OPTIONS LIST AMB0420
SUBROUTINE SOF(ISTOP) AMB0421
IMPLICIT REAL*8(A-H,O-Z) AMB0422
CHARACTER*4 ISTOP(1) AMB0423
COMMON /GAMA/G,G1,G2,G3,G4,G5,G6,G7,G8,G9,G10,G11,G12,G13,G14,G15,AMB0424
1 G16,G17,G18,G19,G20 AMB0425
COMMON /PAR/C0,ENO,EM1,D,SIGMA,TLIM,DRO,ELO,Q0,T0,FACT,ALOGF, AMB0426
1 DPSI0,DTMAX,DETA0,ETALIM,XSI,XSF AMB0427
COMMON /NPAR/NPHI,IPAR,NP,NR,NX,NXS,NS,NSPEC,NS1,NS2,NTAU0,NETAO, AMB0428
1 NAMB,NCASE,ICASE,IFAN AMB0429
COMMON /GEOM/APF,PAI,PAI2,W,SW,CW,BETA,SBETA,CBETA,PSI1,SPSI1, AMB0430
1 CPSI1,PSIF,SPSIF,CPSIF,TPSIF,AK,SK,CK,A0,RF,XF,YF,ZF,AMB0431
2 PHISOF,PHIF,SPHIF,CPHIF,DYMIN,RMIN,XS,DIST,X0,Y0,Z0, AMB0432

```

```

3      DY0, DEG, PSIN, ST1, CT1, OMEGX, OMEGY, OMEGZ, XSV(21)          AMB0433
COMMON /EPSIL/EPSETA,EPST,EPSR                                AMB0434
COMMON /EXTREM/TEXT(5),ETAEXT(5),ETAKXT(5),PHIEXT(5),          AMB0435
1          PSIEXT(5),EMEXT(5),FEXT(5),WEXT(5),                  AMB0436
2          TMAX(5),ETAKMX(5),ETAMAX(5),PSIMAX(5),              AMB0437
3          EMMAX(5),FMAX(5),                                    AMB0438
4          RFMAX(5),PHIFMX(5),PHIMAX(5),WMAX(5)                AMB0439
COMMON /SOFPR/C,DSUMF,DSUMD,T,ETA,DETA,SUM,DSUM,SUMU,DSUMU   AMB0440
COMMON /SUMS/SUMF(5),SUMD(5),SUMU2(5)                           AMB0441
COMMON /COUNTS/ICONTC,ICONTT,ICNTOT,ICNTMX,IQTOT(5),ISHAD(5)  AMB0442
COMMON /SPEC/WAV,XC(5),WC(5),WRC(5),XNAME(5),QFC(5),QDC(5),  AMB0443
1          QU2C(5),FLUXC(5),OMEGA(5),FLXU2C(5),URMSC(5)        AMB0444
PRINT 1,ISTOP                                              AMB0445
1 FORMAT(///1X,2H**,2X,30A4,2X,2H**,///)                    AMB0446
PRINT 71,NS,NP,NR,NX,ICONTC,ICONTT                           AMB0447
71 FORMAT(1X,'NS,NP,NR,NX,ICONTC,ICONTT=',6I6/)            AMB0448
IF(NS.GT.NSPEC) NS=1                                         AMB0449
PRINT 72,RF,PHIF*DEG,PHISOF*DEG,W*DEG,BETA*DEG             AMB0450
72 FORMAT(/1X,'RF,PHIF,PHISOF,W,BETA=',D14.5,4F10.3/)       AMB0451
PRINT 73,C,T,TLIM,ETA                                         AMB0452
73 FORMAT(/1X,'C,T,TLIM,ETA=',4D14.5/)                      AMB0453
PRINT 74,DSUM,SUM,DSUMF,SUMF(NS),SUMD(NS),QDC(NS),QFC(NS),  AMB0454
1          FLUXC(NS),OMEGA(NS)                                AMB0455
74 FORMAT(1X,'DSUM,SUM,DSUMF,SUMF(NS),SUMD(NS)=',5D14.5/     AMB0456
1          1X,'QDC(NS),QFC(NS),FLUXC(NS),OMEGA(NS)=',4D14.5/)  AMB0457
XX=-1.D0                                                       AMB0458
YY=DSQRT(XX)+1.D0                                           AMB0459
STOP                                                       AMB0460
END                                                       AMB0461
SUBROUTINE FLUX                                              AMB0462
IMPLICIT REAL*8(A-H,O-Z)                                     AMB0463
COMMON /GAMA/G,G1,G2,G3,G4,G5,G6,G7,G8,G9,G10,G11,G12,G13,G14,G15,AMB0464
1          G16,G17,G18,G19,G20                                AMB0465
COMMON /PAR/C0,ENO,EM1,D,SIGMA,TLIM,DRO,EL0,Q0,T0,FACT,ALOGF,  AMB0466
1          DPSIO,DTMAX,DETA0,ETALIM,XSI,XSF                 AMB0467
COMMON /NPAR/NPHI,IPAR,NP,NR,NX,NXS,NS,NSPEC,NS1,NS2,NTAU0,NETA0,  AMB0468
1          NAMB,NCASE,ICASE,IFAN                            AMB0469
COMMON /GEOM/APF,PAI,PAI2,W,SW,CW,BETA,SBETA,CBETA,PSI1,SPSI1,  AMB0470
1          CPSI1,PSIF,SPSIF,CPSIF,TPSIF,AK,SK,CK,A0,RF,XF,YF,ZF,AMB0471
2          PHISOF,PHIF,SPHIF,CPHIF,DYMIN,RMIN,XS,DIST,X0,Y0,Z0,  AMB0472
3          DY0,DEG,PSIN,ST1,CT1,OMEGX,OMEGY,OMEGZ,XSV(21)        AMB0473
COMMON /EPSIL/EPSETA,EPST,EPSR                                AMB0474
COMMON /EXTREM/TEXT(5),ETAEXT(5),ETAKXT(5),PHIEXT(5),          AMB0475
1          PSIEXT(5),EMEXT(5),FEXT(5),WEXT(5),                  AMB0476
2          TMAX(5),ETAKMX(5),ETAMAX(5),PSIMAX(5),              AMB0477
3          EMMAX(5),FMAX(5),                                    AMB0478
4          RFMAX(5),PHIFMX(5),PHIMAX(5),WMAX(5)                AMB0479
COMMON /SOFPR/C,DSUMF,DSUMD,T,ETA,DETA,SUM,DSUM,SUMU,DSUMU   AMB0480
COMMON /COUNTS/ICONTC,ICONTT,ICNTOT,ICNTMX,IQTOT(5),ISHAD(5)  AMB0481
COMMON /SPEC/WAV,XC(5),WC(5),WRC(5),XNAME(5),QFC(5),QDC(5),  AMB0482
1          QU2C(5),FLUXC(5),OMEGA(5),FLXU2C(5),URMSC(5)        AMB0483
COMMON /SUMS/SUMF(5),SUMD(5),SUMU2(5)                           AMB0484
EL0=SIGMA*RF*ENO                                             AMB0485
IF(Z0.NE.0.)                                                 AMB0486
1CALL SOF('THE SCHEME HERE IS NOT WRITTEN FOR Z0.NE.0.')    AMB0487
YY0=(Y0-A0)/X0                                               AMB0488
PCHECK=DATAN(YY0)                                           AMB0489
IF(PCHECK.GT.PSIF-1.D-4.OR.PCHECK.LT.-1.D-4)               AMB0490
1CALL SOF('FLUX RECEIVING POINT WITHIN FAN OR WITHIN SPACECRAFT') AMB0491
SPHIF=DSIN(PHIF)                                            AMB0492
CPHIF=DCOS(PHIF)                                           AMB0493
XF=RF*CPSIF                                              AMB0494
YF=APF*CPHIF                                              AMB0495
ZF=APF*SPHIF                                              AMB0496
TBETA=ZF/(YF-Y0)                                           AMB0497
BETA=DATAN(TBETA)                                         AMB0498
IF(DABS(BETA).GT.PAI2) CALL SOF('BETA.GT.PAI/2')           AMB0499
SBETA=DSIN(BETA)                                           AMB0500
CBETA=DCOS(BETA)                                           AMB0501
DIST=DSQRT((XF-X0)**2+(YF-Y0)**2+(ZF-Z0)**2)            AMB0502
CW=(XF-X0)/DIST                                           AMB0503
SW=DSQRT(1.D0-CW**2)                                      AMB0504

```

```

W=PAI2-DATAN(CW/SW) AMB0505
OMEGX=CW AMB0506
OMEGY=SW*CBETA AMB0507
OMEGZ=SW*SBETA AMB0508
CALL LIMIT AMB0509
C DO 20 NS=NS1,NS2 AMB0510
SUMF(NS)=0. AMB0511
SUMU2(NS)=0. AMB0512
SUMD(NS)=0. AMB0513
FEXT(NS)=0. AMB0514
CALL SUMT AMB0515
SUMF(NS)=SUM AMB0516
SUMU2(NS)=SUMU AMB0517
QFC(NS)=SUMF(NS)/FACT AMB0518
QU2C(NS)=SUMU2(NS)/FACT AMB0519
FEXT(NS)=FEXT(NS)/FACT AMB0520
CALL FAN(TEXT(NS),PSIEXT(NS),PHIEXT(NS)) AMB0521
IF(PSIEXT(NS).LT.PSIF-1.D-10) CALL SOF('PSIEXT(NS).LT.PSIF') AMB0522
IF(PSIEXT(NS).GT.PSI1) PSIEXT(NS)=PSI1 AMB0523
PSI0=PSIEXT(NS) AMB0524
T=TEXT(NS) AMB0525
CALL MATCH(T,PSI0,EM,TETA) AMB0526
EMEXT(NS)=EM AMB0527
WEXT(NS)=W AMB0528
IQTOT(NS)=IQTOT(NS)+ICONTT AMB0529
20 CONTINUE AMB0530
RETURN AMB0531
END AMB0532
SUBROUTINE LIMIT AMB0533
IMPLICIT REAL*8(A-H,O-Z) AMB0534
COMMON /GAMA/G,G1,G2,G3,G4,G5,G6,G7,G8,G9,G10,G11,G12,G13,G14,G15,AMB0535
1 G16,G17,G18,G19,G20 AMB0536
COMMON /PAR/C0,ENO,EM1,D,SIGMA,TLIM,DRO,ELO,Q0,T0,FACT,ALOGF, AMB0538
1 DPSI0,DTMAX,DETA0,ETALIM,XSI,XSF AMB0539
COMMON /NPAR/NPHI,IPAR,NP,NR,NX,NXS,NS,NSPEC,NS1,NS2,NTAU0,NETAO, AMB0540
1 NAMB,NCASE,ICASE,IFAN AMB0541
COMMON /GEOM/APF,PAI,PAI2,W,SW,CW,BETA,SBETA,CBETA,PSI1,SPSI1, AMB0542
1 CPSI1,PSI1,SPSIF,CPSIF,TPSIF,AK,SK,CK,A0,RF,XF,YF,ZF,AMB0543
2 PHISOF,PHIF,SPHIF,CPHIF,DYMIN,RMIN,XS,DIST,X0,Y0,Z0, AMB0544
3 DY0,DEG,PSIN,ST1,CT1,OMEGX,OMEGY,OMEGZ,XSV(21) AMB0545
COMMON /EPSIL/EPSETA,EPST,EPSR AMB0546
COMMON /EXTREM/TEXT(5),ETAEXT(5),ETAKXT(5),PHIEXT(5), AMB0547
1 PSIEXT(5),EMEXT(5),FEXT(5),WEXT(5), AMB0548
2 TMAX(5),ETAKMX(5),ETAMAX(5),PSIMAX(5), AMB0549
3 EMMAX(5),FMAX(5), AMB0550
4 RFMAX(5),PHIFMX(5),PHIMAX(5),WMAX(5) AMB0551
COMMON /SPEC/WAV,XC(5),WC(5),WRC(5),XNAME(5),QFC(5),QDC(5), AMB0552
1 QU2C(5),FLUXC(5),OMEGA(5),FLXU2C(5),URMSC(5) AMB0553
AAA=(CW/CPSI1)**2-1.D0 AMB0554
IF(AAA.LT.1.D-10) GO TO 1 AMB0555
TPSI1=SPSI1/CPSI1 AMB0556
AP1=A0+XF*TPSI1 AMB0557
BBB=2.D0*(AP1*CW*TPSI1-SW*APF*(CBETA*CPHIF+SBETA*SPHIF)) AMB0558
CCC=AP1**2-APF**2 AMB0559
DDD=BBB**2-4.D0*AAA*CCC AMB0560
TLIM=(-BBB+DSQRT(DDD))/(2.D0*AAA) AMB0561
TLIM=TLIM/RF AMB0562
RETURN AMB0563
1 CONTINUE AMB0564
TLIM=1.D 55 AMB0565
RETURN AMB0566
END AMB0567
SUBROUTINE SUMT AMB0568
IMPLICIT REAL*8(A-H,O-Z) AMB0569
COMMON /GAMA/G,G1,G2,G3,G4,G5,G6,G7,G8,G9,G10,G11,G12,G13,G14,G15,AMB0570
1 G16,G17,G18,G19,G20 AMB0571
COMMON /PAR/C0,ENO,EM1,D,SIGMA,TLIM,DRO,ELO,Q0,T0,FACT,ALOGF, AMB0572
1 DPSI0,DTMAX,DETA0,ETALIM,XSI,XSF AMB0573
COMMON /NPAR/NPHI,IPAR,NP,NR,NX,NXS,NS,NSPEC,NS1,NS2,NTAU0,NETAO, AMB0574
1 NAMB,NCASE,ICASE,IFAN AMB0575
COMMON /GEOM/APF,PAI,PAI2,W,SW,CW,BETA,SBETA,CBETA,PSI1,SPSI1, AMB0576

```

```

1      CPSI1,PSIF,SPSIF,CPSIF,TPSIF,AK,SK,CK,A0,RF,XF,YF,ZF,AMB0577
2      PHISOF,PHIF,SPHIF,CPHIF,DYMIN,RMIN,XS,DIST,X0,Y0,Z0, AMB0578
3      DY0,DEG,PSIN,ST1,CT1,OMEGX,OMEGY,OMEGZ,XSV(21)        AMB0579
COMMON /EPSIL/EPSETA,EPST,EPSR                           AMB0580
COMMON /EXTREM/TEXT(5),ETAEXT(5),ETAKXT(5),PHIEXT(5),    AMB0581
1      PSIEXT(5),EMEXT(5),FEXT(5),WEXT(5),                AMB0582
2      TMAX(5),ETAKMX(5),ETAMAX(5),PSIMAX(5),            AMB0583
3      EMMAX(5),FMAX(5),                                AMB0584
4      RFMAX(5),PHIFMX(5),PHIMAX(5),WMAX(5)             AMB0585
COMMON /SOFPR/CC,DSUMF,DSUMD,T,ETA,DETA,SUM,DSUM,SUMU,DSUMU   AMB0586
COMMON /COUNTS/ICONTc,ICONTt,ICNTOT,ICNTMX,IQTOT(5),ISHAD(5)  AMB0587
COMMON /SPEC/WAV,XC(5),WC(5),WRCC(5),XNAME(5),QFC(5),QDC(5),  AMB0588
1      QU2C(5),FLUXC(5),OMEGA(5),FLXU2C(5),URMSC(5)       AMB0589
COMMON /SUMS/SUMF(5),SUMD(5),SUMU2(5)                   AMB0590
C INTEGRATION OF FLUX ARRIVING ALONG A SINGLE RAY          AMB0591
DT=DPSI0
PSIN=PSIF
ETA1=0.
ETA3=0.
FETA4=0.
FETAU4=0.
T=0.
SUM=0.
SUMU=0.
ICONTT=0
1      ICONTT=ICONTT+1                                     AMB0602
PSIL=PSIN
DT2=DT/2.D0
DT6=DT/6.D0
T1=T+DT2
T2=T+DT
FETA1=FETA4
FETAU1=FETAU4
CALL PATHK(T1,ETAK1)
CALL FETA(T1,ETA1,ETAK1,GT2,FETA2,FETAU2)           AMB0611
FETA3=FETA2
FETAU3=FETAU2
CALL PATHK(T2,ETAK3)
CALL FETA(T2,ETA3,ETAK3,GT4,FETA4,FETAU4)           AMB0615
DETA=DT*GT4
DSUM=DT6*(FETA1+2.D0*(FETA2+FETA3)+FETA4)          AMB0616
DSUMU=DT6*(FETAU1+2.D0*(FETAU2+FETAU3)+FETAU4)     AMB0618
T=T+DT
ETA=ETA3
ETAK=ETAK3
SUM=SUM+DSUM
SUMU=SUMU+DSUMU
IF(FEXT(NS).GT.FETA4) GO TO 10
FEXT(NS)=FETA4
TEXT(NS)=T
ETAEXT(NS)=ETA
ETAKXT(NS)=ETAK
10     CONTINUE
C STEP CONTROL (DT)
CALL FAN(T,PSI,PHI)
IF(PSI.LT.PSIF-1.D-10) CALL SOF('PSI.LT.PSIF')      AMB0630
IF(PSI.GT.PSIL) PSI=PSI1
PSIN=PSI
DPSI=PSIN-PSIL
DTP=DT*(DPSI0/(DPSI+1.D-10))
DTE=DT*(DETA0/(DETA+1.D-10))
DT1=1.2D0*DT
DT=DMIN1(DTP,DTE,DT1,DTMAX)
IF(DT.LE.0.) CALL SOF('COMPUTED DT NEGATIVE')        AMB0640
15     CONTINUE
IF(IPAR.LT.1)
1PRINT 111,NR,NP,T,PSI*DEG,PHI*DEG,ETA,ETAK,SUM,DSUM/(SUM+1.D-20) AMB0643
111    FORMAT(1X,'NR,NP,T,PSI,PHI=',2I3,3D12.3/          AMB0644
1      1X,'ETA,ETAK,SUM,ERRR=',4D12.3)                 AMB0645
IF(ICONTT.GT.ICNTMX)                                  AMB0646
1CALL SOF('ICONTT TOO LARGE')                      AMB0647
IF(ICONTT.LE.2) GO TO 1                               AMB0648

```

```

IF(ETA+ETAK.GT.ETALIM) GO TO 100 AMB0649
IF(T.GT.50.D0 .OR. T*RF.GT.A0) GO TO 100 AMB0650
IF(SUM.EQ.0.) GO TO 1 AMB0651
ERR=(DSUM/SUM)/DT AMB0652
IF(ERR.GT.EPST) GO TO 1 AMB0653
100 CONTINUE AMB0654
SUM=SUM*EL0 AMB0655
SUMU=SUMU*EL0 AMB0656
RETURN AMB0657
END AMB0658
SUBROUTINE FETA(T,ETAIK,ETAK,GT,FET,FETU2) AMB0659
IMPLICIT REAL*8(A-H,O-Z) AMB0660
REAL*8 MU1,MU2 AMB0661
COMMON /GAMA/G,G1,G2,G3,G4,G5,G6,G7,G8,G9,G10,G11,G12,G13,G14,G15,AMB0662
1 G16,G17,G18,G19,G20 AMB0663
COMMON /PAR/C0,ENO,EM1,D,SIGMA,TLIM,DRO,EL0,Q0,T0,FACT,ALOGF, AMB0664
1 DPSIO,DTMAX,DETA0,ETALIM,XSI,XSF AMB0665
COMMON /NPAR/NPHI,IPAR,NP,NR,NX,NXS,NS,NSPEC,NS1,NS2,NTAU0,NETA0, AMB0666
1 NAMB,NCASE,ICASE,IFAN AMB0667
COMMON /GEOM/APF,PAI,PAI2,W,SW,CW,BETA,SBETA,CBETA,PSI1,SPSI1, AMB0668
1 CPSI1,PSI,SPSIF,CPSIF,TPSIF,AK,SK,CK,A0,RF,XF,YF,ZF,AMB0669
2 PHISOF,PHIF,SPHIF,CPHIF,DYMIN,RMIN,XS,DIST,X0,Y0,Z0,AMB0670
3 DY0,DEG,PSIN,ST1,CT1,OMEGX,OMEGY,OMEGZ,XSV(21) AMB0671
COMMON /EPSIL/EPSETA,EPST,EPSR AMB0672
COMMON /EXTREM/TEXT(5),ETAEKT(5),ETAKXT(5),PHIEXT(5), AMB0673
1 PSIEXT(5),EMEXT(5),FEXT(5),WEXT(5), AMB0674
2 TMAX(5),ETAKMX(5),ETAMAX(5),PSIMAX(5), AMB0675
3 EMMAX(5),FMAX(5), AMB0676
4 RFMAX(5),PHIFMX(5),PHIMAX(5),WMAX(5) AMB0677
COMMON /SPEC/WAV,XC(5),WC(5),WRC(5),XNAME(5),QFC(5),QDC(5), AMB0678
1 QU2C(5),FLUXC(5),OMEGA(5),FLXU2C(5),URMSC(5) AMB0679
COMMON /AMBIEN/ENA,UA,PSIA,PHIA,HA(3),WA(3), AMB0680
1 UAX,UAY,UAZ,AA,BA,CA,RA,XA,YA,ZA,SHADOW AMB0681
LOGICAL SHADOW AMB0682
COMMON /NAGESH/PIK,UIK,UIKX,UIKY,UIKZ AMB0683
ETAIK=0. AMB0684
IF(SHADOW) GO TO 1 AMB0685
K=1 AMB0686
I=NS AMB0687
CALL FAN(T,PSI,PHI) AMB0688
IF(PSI.LT.PSIF-1.D-10) CALL SOF('PSI.LT.PSIF') AMB0689
IF(PSI.GT.PSII) PSI=PSII AMB0690
PSI0=PSI AMB0691
CALL MATCH(T,PSI0,EM,TETA) AMB0692
SPSI=DSIN(PSI) AMB0693
CPSI=DCOS(PSI) AMB0694
SPHI=DSIN(PHI) AMB0695
CPHI=DCOS(PHI) AMB0696
ST=DSIN(TETA) AMB0697
CT=DCOS(TETA) AMB0698
GOREM=1.D0+G1*EM**2 AMB0699
TERMN=GOREM**G6 AMB0700
U=EM*C0/DSQRT(GOREM) AMB0701
UX=U*CT AMB0702
UY=U*ST*CPHI AMB0703
UZ=U*ST*SPHI AMB0704
C COLLISION AMB0705
MU1=WC(I)/(WC(I)+WA(K)) AMB0706
MU2=1.D0-MU1 AMB0707
UMX=MU1*UX+MU2*UAX AMB0708
UMY=MU1*UY+MU2*UAY AMB0709
UMZ=MU1*UZ+MU2*UAZ AMB0710
DOTUM=OMEGX*UMX+OMEGY*UMY+OMEGZ*UMZ AMB0711
URX=UX-UAX AMB0712
URY=UY-UAY AMB0713
URZ=UZ-UAZ AMB0714
UR=DSQRT(URX**2+URY**2+URZ**2) AMB0715
DET=DOTUM**2+(MU2*UR)**2-(UMX**2+UMY**2+UMZ**2) AMB0716
IF(DET.LT.0.) GO TO 1 AMB0717
DET1=DSQRT(DET) AMB0718
UIK1=-DOTUM+DET1 AMB0719
UIK2=-DOTUM-DET1 AMB0720

```

```

IF(UIK2.GT.0.) CALL SOF('DOUBLE COLLISION OPTION NOT PROGRAMMED') AMB0721
1 YET') AMB0722
UIK=UIK1 AMB0723
IF(UIK.LE.0.) GO TO 1 AMB0724
UIKX=-OMEGX*UIK AMB0725
UIKY=-OMEGY*UIK AMB0726
UIKZ=-OMEGZ*UIK AMB0727
CDEL=(DOTUM+UIK)/(MU2*UR) AMB0728
IF(CDEL.LE.0.) CALL SOF('CDEL NEGATIVE NOT PROGRAMMED YET') AMB0729
IF(CDEL-1.D-10.GT.1.D0) AMB0730
1CALL SOF('CDEL (COS(DELTA)) CANNOT BE GT.1.') AMB0731
PIK=(UIK/(MU2*UR))**2/(4.D0*PAI*CDEL) AMB0732
IF (PIK.LT.0.) CALL SOF('PIK.LT.0') AMB0733
FET=(UR/UA)*PIK/TERMN AMB0734
UREL=DSQRT((UX-UIKX)**2+(UY-UIKY)**2+(UZ-UIKZ)**2) AMB0735
GT=EL0*(UREL/UIK)/TERMN AMB0736
CALL PATHIK(T,ETAIK) AMB0737
POWER=ETAIK+ETAK-ALOGF AMB0738
EFACT=0. AMB0739
IF(POWER.LT.60.D0)EFACT=DEXP(-POWER) AMB0740
FET=FET*EFACT AMB0741
FETU2=FET*UIK**2 AMB0742
IF(EM.LT.0.) CALL SOF('EM.LT.0') AMB0743
FETU2=FET*EM AMB0744
RETURN AMB0745
1 CONTINUE AMB0746
FET=0. AMB0747
FETU2=0. AMB0748
GT=0. AMB0749
RETURN AMB0750
END AMB0751
SUBROUTINE PATHIK(TC,ETAIK) AMB0752
IMPLICIT REAL*8(A-H,O-Z) AMB0753
REAL*8 MU1,MU2 AMB0754
COMMON /GAMA/G,G1,G2,G3,G4,G5,G6,G7,G8,G9,G10,G11,G12,G13,G14,G15,AMB0755
1 G16,G17,G18,G19,G20 AMB0756
COMMON /PAR/C0,ENO,EM1,D,SIGMA,TLIM,DR0,EL0,Q0,T0,FACT,ALOGF, AMB0757
1 DPSIO,DTMAX,DETA0,ETALIM,XSI,XSF AMB0758
COMMON /NPAR/NPHI,IPAR,NP,NR,NX,NXS,NS,NSPEC,NS1,NS2,NTAU0,NETAO, AMB0759
1 NAMB,NCASE,ICASE,IFAN AMB0760
COMMON /GEOM/APF,PAI,PAI2,W,SW,CW,BETA,SBETA,CBETA,PSI1,SPSI1, AMB0761
1 CPSI1,PSIF,SPSIF,CPSIF,TPSIF,AK,SK,CK,A0,RF,XF,YF,ZF,AMB0762
2 PHISOF,PHIF,SPHIF,CPHIF,DYMIN,RMIN,XS,DIST,X0,Y0,Z0, AMB0763
3 DY0,DEG,PSIN,ST1,CT1,OMEGX,OMEGY,OMEGZ,XSV(21) AMB0764
COMMON /EPSIL/EPSETA,EPST,EPSSR AMB0765
COMMON /EXTREM/TEXT(5),ETAKXT(5),PHIEXT(5), AMB0766
1 PSIEXT(5),EMEXT(5),FEXT(5),WEXT(5), AMB0767
2 TMAX(5),ETAKMX(5),ETAMAX(5),PSIMAX(5), AMB0768
3 EMMAX(5),FMAX(5), AMB0769
4 RFMAX(5),PHIFMX(5),PHIMAX(5),WMAX(5) AMB0770
COMMON /SPEC/WAV,XC(5),WC(5),WRC(5),XNAME(5),QFC(5),QDC(5), AMB0771
1 QU2C(5),FLUXC(5),OMEGA(5),FLXU2C(5),URMSC(5) AMB0772
COMMON /AMBIEN/ENA,UA,PSIA,PHIA,HA(3),WA(3), AMB0773
1 UAX,UAY,UAZ,AA,BA,CA,RA,XA,YA,ZA,SHADOW AMB0774
LOGICAL SHADOW AMB0775
NETA=NETAO AMB0776
DT=TC/DBLE(NETA) AMB0777
DT2=DT/2.D0 AMB0778
DT6=DT/6.D0 AMB0779
GT4=0. AMB0780
T=0. AMB0781
ETA=0. AMB0782
IT=0 AMB0783
1 IT=IT+1 AMB0784
T1=T+DT2 AMB0785
T2=T+DT AMB0786
GT1=GT4 AMB0787
CALL FT(T1,GT2) AMB0788
GT3=GT2 AMB0789
CALL FT(T2,GT4) AMB0790
DETA=DT6*(GT1+2.D0*(GT2+GT3)+GT4) AMB0791
T=T+DT AMB0792

```

```

ETA=ETA+DETA          AMB0793
IF(IT.LT.NETA) GO TO 1 AMB0794
ETAIK=ETA             AMB0795
RETURN                AMB0796
END                  AMB0797
SUBROUTINE FT(T,GT)   AMB0798
IMPLICIT REAL*8(A-H,0-Z) AMB0799
REAL*8 MU1,MU2        AMB0800
COMMON /GAMA/G,G1,G2,G3,G4,G5,G6,G7,G8,G9,G10,G11,G12,G13,G14,G15,AMB0801
1           G16,G17,G18,G19,G20          AMB0802
COMMON /PAR/C0,ENO,EM1,D,SIGMA,TLIM,DR0,EL0,Q0,T0,FACT,ALOGF,      AMB0803
1           DPSI0,DTMAX,DETA0,ETALIM,XSI,XSF          AMB0804
COMMON /NPAR/NPHI,IPAR,NP,NR,NX,NXS,NS,NSPEC,NS1,NS2,NTAU0,NETAO, AMB0805
1           NAMB,NCASE,ICASE,IFAN          AMB0806
COMMON /GEOM/APF,PAI,PAI2,W,SW,CW,BETA,CBETA,PSI1,SPSI1,      AMB0807
1           CPSI1,PSIF,SPSIF,CPSIF,TPSIF,AK,SK,CK,A0,RF,XF,YF,ZF,AMB0808
2           PHISOF,PHIF,SPHIF,CPHIF,DYMIN,RMIN,XS,DIST,X0,Y0,Z0,AMB0809
3           DY0,DEG,PSIN,ST1,CT1,OMEGX,OMEGY,OMEGZ,XSV(21)          AMB0810
COMMON /EPSIL/EPSETA,EPST,EPSR          AMB0811
COMMON /EXTREM/TEXT(5),ETAEXT(5),ETAKXT(5),PHIEXT(5),          AMB0812
1           PSIEXT(5),EMEXT(5),FEXT(5),WEXT(5),          AMB0813
2           TMAX(5),ETAKMX(5),ETAMAX(5),PSIMAX(5),          AMB0814
3           EMAX(5),FMAX(5),          AMB0815
4           RFMAX(5),PHIFMX(5),PHIMAX(5),WMAX(5)          AMB0816
COMMON /SPEC/WAV,XC(5),WC(5),WRC(5),XNAME(5),QFC(5),QDC(5),      AMB0817
1           QU2C(5),FLUXC(5),OMEGA(5),FLXU2C(5),URMSC(5)          AMB0818
COMMON /AMBIEN/ENA,UA,PSIA,PHIA,HA(3),WA(3),          AMB0819
1           UAX,UAY,UAZ,AA,BA,CA,RA,XA,YA,ZA,SHADOW          AMB0820
LOGICAL SHADOW          AMB0821
COMMON /NAGESH/PIK,UIK,UIKX,UIKY,UIKZ          AMB0822
K=1          AMB0823
I=NS          AMB0824
CALL FAN(T,PSI,PHI)          AMB0825
IF(PSI.LT.PSIF-1.D-10) CALL SOF('PSI.LT.PSIF')          AMB0826
IF(PSI.GT.PSI1) PSI=PSI1          AMB0827
PSI0=PSI          AMB0828
CALL MATCH(T,PSI0,EM,TETA)          AMB0829
SPSI=DSIN(PSI)          AMB0830
CPSI=DCOS(PSI)          AMB0831
SPHI=DSIN(PHI)          AMB0832
CPHI=DCOS(PHI)          AMB0833
ST=DSIN(TETA)          AMB0834
CT=DCOS(TETA)          AMB0835
GOREM=1.D0+G1*EM**2          AMB0836
TERMN=GOREM**G6          AMB0837
U=EM*CO/DSQRT(GOREM)          AMB0838
UX=U*CT          AMB0839
UY=U*ST*CPHI          AMB0840
UZ=U*ST*SPHI          AMB0841
UREL=DSQRT((UX-UIKX)**2+(UY-UIKY)**2+(UZ-UIKZ)**2)          AMB0842
GT=EL0*(UREL/UIK)/TERMN          AMB0843
RETURN          AMB0844
END          AMB0845
SUBROUTINE PATHK(T,ETAK)          AMB0846
IMPLICIT REAL*8(A-H,0-Z)          AMB0847
COMMON /GAMA/G,G1,G2,G3,G4,G5,G6,G7,G8,G9,G10,G11,G12,G13,G14,G15,AMB0848
1           G16,G17,G18,G19,G20          AMB0849
COMMON /PAR/C0,ENO,EM1,D,SIGMA,TLIM,DR0,EL0,Q0,T0,FACT,ALOGF,      AMB0850
1           DPSI0,DTMAX,DETA0,ETALIM,XSI,XSF          AMB0851
COMMON /NPAR/NPHI,IPAR,NP,NR,NX,NXS,NS,NSPEC,NS1,NS2,NTAU0,NETAO, AMB0852
1           NAMB,NCASE,ICASE,IFAN          AMB0853
COMMON /GEOM/APF,PAI,PAI2,W,SW,CW,BETA,CBETA,PSI1,SPSI1,      AMB0854
1           CPSI1,PSIF,SPSIF,CPSIF,TPSIF,AK,SK,CK,A0,RF,XF,YF,ZF,AMB0855
2           PHISOF,PHIF,SPHIF,CPHIF,DYMIN,RMIN,XS,DIST,X0,Y0,Z0,AMB0856
3           DY0,DEG,PSIN,ST1,CT1,OMEGX,OMEGY,OMEGZ,XSV(21)          AMB0857
COMMON /EPSIL/EPSETA,EPST,EPSR          AMB0858
COMMON /EXTREM/TEXT(5),ETAEXT(5),ETAKXT(5),PHIEXT(5),          AMB0859
1           PSIEXT(5),EMEXT(5),FEXT(5),WEXT(5),          AMB0860
2           TMAX(5),ETAKMX(5),ETAMAX(5),PSIMAX(5),          AMB0861
3           EMAX(5),FMAX(5),          AMB0862
4           RFMAX(5),PHIFMX(5),PHIMAX(5),WMAX(5)          AMB0863
COMMON /COUNTS/ICONTC,ICONTT,ICNTOT,ICNTMX,IQTOT(5),ISHAD(5)          AMB0864

```

```

COMMON /AMBIEN/ENA,UA,PSIA,PHIA,HA(3),WA(3),
1          UAX,UAY,UAZ,AA,BA,CA,RA,XA,YA,ZA,SHADOW      AMB0865
LOGICAL SHADOW                                     AMB0866
ETAK=0.                                              AMB0867
C DETERMINE POINT OF ENTRY OF AMBIENT TRAJECTORY TO FAN   AMB0868
TRF=T*RF                                           AMB0869
XC=XF+TRF*OMEGX                                    AMB0870
YC=YF+TRF*OMEGY                                    AMB0871
ZC=ZF+TRF*OMEGZ                                    AMB0872
C CHECK SHADOW                                     AMB0873
SHADOW=.FALSE.                                     AMB0874
EVER=BA**2+CA**2                                    AMB0875
DETS=EVER*A0**2-(BA*ZC-CA*YC)**2                  AMB0876
IF(DETS.LE.0.) GO TO 2                            AMB0877
DETS1=DSQRT(DETS)                                 AMB0878
TAU1=(-(BA*YC+CA*ZC)+DETS1)/EVER                AMB0879
IF(TAU1.GT.0.) SHADOW=.TRUE.                      AMB0880
2 CONTINUE                                         AMB0881
IF(SHADOW) GO TO 10                               AMB0882
EVER1=A0+XC*TPSIF                                AMB0883
EVER2=BA**2+CA**2-(AA*TPSIF)**2                  AMB0884
EVER3=BA*YC+CA*ZC-AA*EVER1*TPSIF                 AMB0885
DET=EVER3**2-EVER2*(YC**2+ZC**2-EVER1**2)       AMB0886
IF(DET.LE.0.)                                       AMB0887
1CALL SOF('NO INTERSECTION OF AMB. TRAJ. WITH LIMITING CONE') AMB0888
DET1=DSQRT(DET)                                 AMB0889
TAUP=(-EVER3+DET1)/EVER2                         AMB0890
TAUM=(-EVER3-DET1)/EVER2                         AMB0891
IF(TAUP.GT.0. .AND. TAUM.GT.0.)                   AMB0892
1CALL SOF('TWO POSITIVE INTERSECTIONS WITH LIMITING CONE NOT PERMIT' AMB0893
1 IN THIS VERSION')                               AMB0894
TAUF=DMAX1(TAUP,TAUM)                           AMB0895
IF(TAUF.LE.0.)                                     AMB0896
1CALL SOF('NO POSITIVE INTERSECTION WITH LIMITING CONE') AMB0897
XA=XC+TAUF*AA                                    AMB0898
YA=YC+TAUF*BA                                    AMB0899
ZA=ZC+TAUF*CA                                    AMB0900
RA=DSQRT(XA**2+(DSQRT(YA**2+ZA**2)-A0)**2)    AMB0901
TAUF=TAUF/RA                                     AMB0902
NTAU=NTAU0                                       AMB0903
DTAU=TAUF/DBLE(NTAU)                           AMB0904
ETAK=0.                                            AMB0905
TAU=0.                                             AMB0906
DTAU2=DTAU/2.D0                                  AMB0907
DTAU6=DTAU/6.D0                                  AMB0908
GTAU4=0.                                           AMB0909
ITAU=0.                                            AMB0910
1 ITAU=ITAU+1                                    AMB0911
TAU1=TAU+DTAU2                                  AMB0912
TAU2=TAU+DTAU                                  AMB0913
GTAU1=GTAU4                                     AMB0914
CALL FTAU(TAU1,GTAU2)                           AMB0915
GTAU3=GTAU2                                     AMB0916
CALL FTAU(TAU2,GTAU4)                           AMB0917
DETAK=DTAU6*(GTAU1+2.D0*(GTAU2+GTAU3)+GTAU4)  AMB0918
TAU=TAU+DTAU                                     AMB0919
ETAK=ETAK+DETAK                                 AMB0920
IF(ITAU.LT.NTAU) GO TO 1                        AMB0921
ETAK=ETAK*(SIGMA*EN0*RA)                         AMB0922
RETURN                                            AMB0923
10 CONTINUE                                         AMB0924
ISHAD(NS)=ISHAD(NS)+1                           AMB0925
RETURN                                            AMB0926
END                                               AMB0927
SUBROUTINE FTAU(TAU,GTAU)                         AMB0928
IMPLICIT REAL*8(A-H,O-Z)                         AMB0929
COMMON /GAMA/G,G1,G2,G3,G4,G5,G6,G7,G8,G9,G10,G11,G12,G13,G14,G15,AMB0930
1          G16,G17,G18,G19,G20                     AMB0931
COMMON /PAR/C0,EN0,EM1,D,SIGMA,TLIM,DR0,ELO,Q0,T0,FACT,ALOGF,  AMB0932
1          DPSI0,DTMAX,DETA0,ETALIM,XSI,XSF        AMB0933
COMMON /NPAR/NPHI,IPAR,NP,NR,NX,NXS,NS,NSPEC,NS1,NS2,NTAU0,NETA0,  AMB0934
1          NAMB,NCASE,IFAN                         AMB0935
1

```

```

COMMON /GEOM/APF,PAI,PAI2,W,SW,CW,BETA,SBETA,CBETA,PSI1,SPSI1, AMB0937
1 CPSI1,PSIF,SPSIF,CPSIF,TPSIF,AK,SK,CK,A0,RF,XF,YF,ZF,AMB0938
2 PHISOF,PHIF,SPHIF,CPHIF,DYMIN,RMIN,XS,DIST,X0,Y0,Z0, AMB0939
3 DY0,DEG,PSIN,ST1,CT1,OMEGX,OMEGY,OMEGZ,XSV(21) AMB0940
COMMON /EPSIL/EPSETA,EPST,EPSR AMB0941
COMMON /EXTREM/TEXT(5),ETAEXT(5),ETAKXT(5),PHIEXT(5), AMB0942
1 PSIEXT(5),EMEXT(5),FEXT(5),WEXT(5), AMB0943
2 TMAX(5),ETAKMX(5),ETAMAX(5),PSIMAX(5), AMB0944
3 EMMAX(5),FMAX(5), AMB0945
4 RFMAX(5),PHIFMX(5),PHIMAX(5),WMAX(5) AMB0946
COMMON /SPEC/WAV,XC(5),WC(5),WRC(5),XNAME(5),QFC(5),QDC(5), AMB0947
1 QU2C(5),FLUXC(5),OMEGA(5),FLXU2C(5),URMSC(5) AMB0948
COMMON /AMBIEN/ENA,UA,PSIA,PHIA,HA(3),WA(3), AMB0949
1 UAX,UAY,UAZ,AA,BA,CA,RA,XA,YA,ZA,SHADOW AMB0950
LOGICAL SHADOW AMB0951
CALL FANT(TAU,PSI,PHI)
IF(PSI.LT.PSIF-1.D-10) CALL SOF('PSI.LT.PSIF') AMB0952
IF(PSI.GT.PSI1) PSI=PSI1 AMB0953
PSI0=PSI AMB0954
CALL MATCH(CT,PSI0,EM,TETA) AMB0955
SPSI=DSIN(PSI) AMB0956
CPSI=DCOS(PSI) AMB0957
SPHI=DSIN(PHI) AMB0958
CPHI=DCOS(PHI) AMB0959
ST=DSIN(TETA) AMB0960
CT=DCOS(TETA) AMB0961
GOREM=1.D0+G1*EM**2 AMB0962
TERMN=GOREM**G6 AMB0963
U=EM*C0/DSQRT(GOREM) AMB0964
UREL=DSQRT((CT*U-UAX)**2+(ST*CPHI*U-UAY)**2+(ST*SPHI*U-UAZ)**2) AMB0965
GTAU=UREL/(UA*TERMN) AMB0966
GTAU=UREL/(UA*TERMN) AMB0967
RETURN AMB0968
END AMB0969
SUBROUTINE FAN(T,PSI,PHI) AMB0970
IMPLICIT REAL*8(A-H,O-Z) AMB0971
COMMON /PAR/C0,ENO,EM1,D,SIGMA,TLIM,DR0,EL0,Q0,T0,FACT,ALOGF, AMB0972
1 DPSI0,DTMAX,DETA0,ETALIM,XSI,XSF AMB0973
COMMON /GEOM/APF,PAI,PAI2,W,SW,CW,BETA,SBETA,CBETA,PSI1,SPSI1, AMB0974
1 CPSI1,PSIF,SPSIF,CPSIF,TPSIF,AK,SK,CK,A0,RF,XF,YF,ZF,AMB0975
2 PHISOF,PHIF,SPHIF,CPHIF,DYMIN,RMIN,XS,DIST,X0,Y0,Z0, AMB0976
3 DY0,DEG,PSIN,ST1,CT1,OMEGX,OMEGY,OMEGZ,XSV(21) AMB0977
COMMON /POINT/XP,YP,XCOR,YCOR AMB0978
C RING FAN GEOMETRY. FAN CORNER IS AT (0,A0*COS(PHI),A0*SIN(PHI)). AMB0979
C RF -- RADIAL DISTANCE ON LIMITING CHARACTERISTIC OF POINT OF AMB0980
C ENTRANCE OF RAY. AMB0981
C DIRECTION COSINES OF RAY: OMEGX,OMEGY,OMEGZ AMB0982
TRF=T*RF AMB0983
X=XF+TRF*OMEGX AMB0984
Y=YF+TRF*OMEGY AMB0985
Z=ZF+TRF*OMEGZ AMB0986
DY=DSQRT(Y*Y+Z*Z)-A0 AMB0987
IF(DABS(DY).LE.1.D-10*A0) DY=1.D-10*A0 AMB0988
IF(DY.LT.0.) AMB0989
1 CALL SOF('POINT X,Y,X CANNOT BE CLOSER TO X-AXIS THAN RADIUS A0') AMB0990
YY=X/DY AMB0991
PSI=PAI2-DATAN(YY) AMB0992
PHI=DATAN(Z/Y) AMB0993
XP=XCOR+X AMB0994
YP=A0+DY AMB0995
RETURN AMB0996
END AMB0997
SUBROUTINE FANT(TAU,PSI,PHI) AMB0998
IMPLICIT REAL*8(A-H,O-Z) AMB0999
COMMON /PAR/C0,ENO,EM1,D,SIGMA,TLIM,DR0,EL0,Q0,T0,FACT,ALOGF, AMB1000
1 DPSI0,DTMAX,DETA0,ETALIM,XSI,XSF AMB1001
COMMON /GEOM/APF,PAI,PAI2,W,SW,CW,BETA,SBETA,CBETA,PSI1,SPSI1, AMB1002
1 CPSI1,PSIF,SPSIF,CPSIF,TPSIF,AK,SK,CK,A0,RF,XF,YF,ZF,AMB1003
2 PHISOF,PHIF,SPHIF,CPHIF,DYMIN,RMIN,XS,DIST,X0,Y0,Z0, AMB1004
3 DY0,DEG,PSIN,ST1,CT1,OMEGX,OMEGY,OMEGZ,XSV(21) AMB1005
COMMON /AMBIEN/ENA,UA,PSIA,PHIA,HA(3),WA(3), AMB1006
1 UAX,UAY,UAZ,AA,BA,CA,RA,XA,YA,ZA,SHADOW AMB1007
COMMON /POINT/XP,YP,XCOR,YCOR AMB1008

```

```

LOGICAL SHADOW AMB1009
C RING FAN GEOMETRY. FAN CORNER IS AT (0,A0*COS(PHI),A0*SIN(PHI)). AMB1010
C RA -- RADIAL DISTANCE ON LIMITING CHARACTERISTIC OF POINT OF AMB1011
C ENTRANCE OF RAY. AMB1012
C DIRECTION COSINES OF RAY: -AA,-BA,-CA AMB1013
TRA=TAU*RA AMB1014
X=XA-TRA*AA AMB1015
Y=YA-TRA*BA AMB1016
Z=ZA-TRA*CA AMB1017
DY=DSQRT(Y*Y+Z*Z)-A0 AMB1018
IF(DABS(DY).LE.1.D-10*A0) DY=1.D-10*A0 AMB1019
IF(DY.LT.0.) AMB1020
1CALL SOF('POINT X,Y,Z CANNOT BE CLOSER TO X-AXIS THAN RADIUS A0') AMB1021
YY=X/DY AMB1022
PSI=PAI2-DATAN(YY) AMB1023
PHI=DATAN(Z/Y) AMB1024
XP=XCOR+X AMB1025
YP=A0+DY AMB1026
RETURN AMB1027
END AMB1028
SUBROUTINE HMSET AMB1029
C SUBROUTINE NUMBER 20 AMB1030
IMPLICIT REAL*8(A-H,O-Z,$) AMB1031
REAL*8 KAPA0B,MHINV,MINV0,M,MF,M1,M2,M3,NORM,MEXIT,LAMDOB AMB1032
COMMON /GAMA/G,G1,G2,G3,G4,G5,G6,G7,G8,G9,G10,G11,G12,G13,G14,G15,AMB1033
1 G16,G17,G18,G19,G20 AMB1034
COMMON /PAR/C0,ENO,EM1,D,SIGMA,TLIM,DRO,ELO,Q0,T0,FACT,ALOGF, AMB1035
1 DPSI0,DTMAX,DETA0,ETALIM,XSI,XSF AMB1036
COMMON /GEOM/APF,PAI,PAI2,W,SW,CW,BETA,SBETA,CBETA,PSI1,SPSI1, AMB1037
1 CPSI1,PSIF,SPSIF,CPSIF,TPSIF,AK,SK,CK,A0,RF,XF,YF,ZF,AMB1038
2 PHISOF,PHIF,SPHIF,CPHIF,DYMIN,RMIN,XS,DIST,X0,Y0,Z0, AMB1039
3 DY0,DEG,PSIN,ST1,CT1,OMEGX,OMEGY,OMEGZ,XSV(21) AMB1040
COMMON /GRP/DMINV,MHINV(101),HMV(101) AMB1041
COMMON /IGRP/KHM AMB1042
C A ROUTINE FOR THE C+ DERIVATIVE DUE TO RING SYMMETRY (GRP). AMB1043
MEXIT=EM1 AMB1044
KHM=51 AMB1045
IF(KHM.GT.101) CALL SOF('2001') AMB1046
MINV0=1.D0/MEXIT AMB1047
DMINV=MINV0/DBLE(KHM-1) AMB1048
M=MEXIT AMB1049
SUM=0. AMB1050
KHM1=KHM-1 AMB1051
DO 1 I=1,KHM1 AMB1052
MF=M AMB1053
MHINV(I)=MINV0-DBLE(I-1)*DMINV AMB1054
M=1.D0/MHINV(I) AMB1055
DM=M-MF AMB1056
M1=M-DM AMB1057
M2=M-DM/2.D0 AMB1058
M3=M AMB1059
CALL MFUNC(M1,F1,ETALF1,TETA1) AMB1060
CALL MFUNC(M2,F2,ETALF2,TETA2) AMB1061
CALL MFUNC(M3,F3,ETALF3,TETA3) AMB1062
SUM=SUM+DM*(F1+4.D0*F2+F3)/6.D0 AMB1063
ETALF=ETALF3 AMB1064
TETA=TETA3 AMB1065
PSI=TETA+DASIN(1.D0/M) AMB1066
NORM=((3.D0-G)/4.D0)*(M**2-1.D0)**0.75D0/ AMB1067
1 (DSIN(PSI)*(1.D0+G1*M**2)**G14) AMB1068
HM=SUM*NORM AMB1069
HMV(I)=HM AMB1070
GOREM=1.D0+G1*M**2 AMB1071
GOR=M**2-1.D0 AMB1072
DELTOB=0.5D0*DSQRT(GOR)*(1.D0/(MEXIT*ETALF) AMB1073
1 +DSIN(TETA)/M)/DSIN(PSI)+G15*HM/2.D0 AMB1074
EPSI0B=DELTOB/DSQRT(GOR)-DSIN(TETA)/(M*DSIN(PSI)) AMB1075
KAPA0B=1.D0 AMB1076
IF(DABS(PAI2-TETA).GT.1.D-6) AMB1077
1 KAPA0B=DTAN(TETA)*EPSI0B AMB1078
LAMDOB=EPSI0B-DELTOB*GOREM/(GOR*DSQRT(GOR)) AMB1079
PRINT 11,I,M,HM,TETA*DEG,PSI*DEG AMB1080

```

```

11 FORMAT(/1X,'I,M,HM,TETA,PSI=',I5,5D12.4) AMB1081
PRINT 12,DELT0B,EPSI0B*DEG,KAPA0B*DEG,LAMDOB*DEG AMB1082
12 FORMAT( 1X,'DELT0B,EPSI0B,KAPA0B,LAMDOB=',5X,5D12.4) AMB1083
1 CONTINUE AMB1084
MHINV(KHM)=0. AMB1085
HMV(KHM)=1.D0 AMB1086
RETURN AMB1087
END AMB1088
SUBROUTINE MFUNC(M,F,ETALF,TETA) AMB1089
C SUBROUTINE NUMBER 21 AMB1090
IMPLICIT REAL*8(A-H,O-Z,$) AMB1091
REAL*8 NU,NUFUNC,M,MEXIT,MD,MDD AMB1092
COMMON /GAMA/G,G1,G2,G3,G4,G5,G6,G7,G8,G9,G10,G11,G12,G13,G14,G15,AMB1093
1 G16,G17,G18,G19,G20 AMB1094
COMMON /PAR/C0,ENO,EM1,D,SIGMA,TLIM,DR0,EL0,Q0,T0,FACT,ALOGF, AMB1095
1 DPSI0,DTMAX,DETA0,ETALIM,XSI,XSF AMB1096
COMMON /GEOM/APF,PAI,PAI2,W,SW,CW,BETA,SBETA,CBETA,PSI1,SPSI1, AMB1097
1 CPSI1,PSIF,SPSIF,CPSIF,TPSIF,AK,SK,CK,A0,RF,XF,YF,ZF,AMB1098
2 PHISOF,PHIF,SPHIF,CPHIF,DYMIN,RMIN,XS,DIST,X0,Y0,Z0, AMB1099
3 DY0,DEG,PSIN,ST1,CT1,OMEGX,OMEGY,OMEGZ,XSV(21) AMB1100
C QF(MDD)=1.D0/DSQRT(MDD**2-1.D0) AMB1101
NUFUNC(MD)=-G5*DATAN(G5*QF(MD))+DATAN(QF(MD)) AMB1102
C MEXIT=EM1 AMB1103
NU=NUFUNC(M) AMB1104
TETA=NUFUNC(MEXIT)+PAI2-NU AMB1105
GOREM=1.D0+G1*M**2 AMB1106
GOR=M**2-1.D0 AMB1107
F=(M**2)*(GOREM**G13)*DSIN(TETA)/GOR**1.25D0 AMB1108
GOREM1=1.D0+G1*MEXIT**2 AMB1109
GOR1=MEXIT**2-1.D0 AMB1110
ETALF=((GOREM/GOREM1)**G14)*((GOR1/GOR)**0.25D0) AMB1111
RETURN AMB1112
END AMB1113
SUBROUTINE HINTER(M,H) AMB1114
C SUBROUTINE NUMBER 22 AMB1115
IMPLICIT REAL*8(A-H,O-Z,$) AMB1116
REAL*8 MINV,M,MEXIT,MHINV AMB1117
COMMON /GAMA/G,G1,G2,G3,G4,G5,G6,G7,G8,G9,G10,G11,G12,G13,G14,G15,AMB1118
1 G16,G17,G18,G19,G20 AMB1119
COMMON /PAR/C0,ENO,EM1,D,SIGMA,TLIM,DR0,EL0,Q0,T0,FACT,ALOGF, AMB1120
1 DPSI0,DTMAX,DETA0,ETALIM,XSI,XSF AMB1121
COMMON /GRP/DMINV,MHINV(101),HMV(101) AMB1122
COMMON /IGRP/KHM AMB1123
C COMPUTE H(M) BY INTERPOLATION AMB1124
MEXIT=EM1 AMB1125
MINV=1.D0/M AMB1126
I=KHM-IDINT(MINV/DMINV-1.D-9)-1 AMB1127
IF(I.GE.1.AND.I.LT.KHM) GO TO 1 AMB1128
PRINT 11,I,KHM,M,MEXIT AMB1129
11 FORMAT(/1X,'I,KHM,M,MEXIT=',2I5,2D14.6/) AMB1130
CALL SOF('2201') AMB1131
1 CONTINUE AMB1132
F1=(MINV-MHINV(I+1))/DMINV AMB1133
F2=1.D0-F1 AMB1134
IF(F1.LT.-1.D-9) CALL SOF('2210') AMB1135
IF(F2.LT.-1.D-9) CALL SOF('2211') AMB1136
H=F1*HMV(I)+F2*HMV(I+1) AMB1137
RETURN AMB1138
END AMB1139
SUBROUTINE MATCH(T,PSI0,MAB,TETAAB) AMB1140
C SUBROUTINE NUMBER 23 AMB1141
IMPLICIT REAL*8(A-H,O-Z,$) AMB1142
REAL*8 M,M0B,MEXIT,MAB,LAMDOB,KAPA0B AMB1143
COMMON /GAMA/G,G1,G2,G3,G4,G5,G6,G7,G8,G9,G10,G11,G12,G13,G14,G15,AMB1144
1 G16,G17,G18,G19,G20 AMB1145
COMMON /PAR/C0,ENO,EM1,D,SIGMA,TLIM,DR0,EL0,Q0,T0,FACT,ALOGF, AMB1146
1 DPSI0,DTMAX,DETA0,ETALIM,XSI,XSF AMB1147
COMMON /NPAR/NPHI,IPAR,NP,NR,NX,NXS,NS,NSPEC,NS1,NS2,NTAU0,NETAO, AMB1148
1 NAMB,NCASE,ICASE,IFAN AMB1149
COMMON /GEOM/APF,PAI,PAI2,W,SW,CW,BETA,SBETA,CBETA,PSI1,SPSI1, AMB1150
1 AMB1151

```

```

1           CPSI1,PSIF,SPSIF,CPSIF,TPSIF,AK,SK,CK,A0,RF,XF,YF,ZF,AMB1153
2           PHISOF,PHIF,SPHIF,CPHIF,DYMIN,RMIN,XS,DIST,X0,Y0,Z0, AMB1154
3           DY0,DEG,PSIN,ST1,CT1,OMEGX,OMEGY,OMEGZ,XSV(21)          AMB1155
COMMON /POINT/XP,YP,XCOR,YCOR                                         AMB1156
COMMON /GRP/DMINV,MHINV(101),HMV(101)                                AMB1157
COMMON /IGRP/KHM                                         AMB1158
MEXIT=EM1                                         AMB1159
GO TO (101,102),IFAN                                         AMB1160
101 CONTINUE                                         AMB1161
C FAN APPROXIMATED AS PLANAR                                         AMB1162
MAB=DSQRT(1.D0+G4/DTAN((PSI0-PSIF)/G5)**2)                         AMB1163
TETAAB=PSI0-DASIN(1.D0/MAB)                                         AMB1164
GO TO 100                                         AMB1165
102 CONTINUE                                         AMB1166
C COMPUTE MAB FROM THE INVERSE PROBLEM SOLUTION                      AMB1167
COTAV=1.D0/DTAN(PSI0)                                         AMB1168
EVY=YP*DLOG(YP/YCOR)/(YP-YCOR)-1.D0                               AMB1169
PSIN=PSI0                                         AMB1170
DO 1 ITER=1,10                                         AMB1171
PSI=PSIN                                         AMB1172
M=DSQRT(1.D0+G4/DTAN((PSI-PSIF)/G5)**2)                         AMB1173
M=DMAX1(M,MEXIT)                                         AMB1174
CALL HINTER(M,HM)                                         AMB1175
CALL MFUNC(M,F,ETALF,TETA)                                         AMB1176
GOREM=1.D0+G1*M**2                                         AMB1177
GOR=M**2-1.D0                                         AMB1178
DELTOB=0.5D0*DSQRT(GOR)*(1.D0/(MEXIT*ETALF))                     AMB1179
1           +DSIN(TETA)/M)/DSIN(PSI)+G15*HM/2.D0                  AMB1180
EPSI0B=DELTOB/DSQRT(GOR)-DSIN(TETA)/(M*DSIN(PSI))                 AMB1181
LAMDOB=EPSI0B-DELTOB*GOREM/(GOR*DSQRT(GOR))                      AMB1182
COTN=COTAV+LAMDOB*EVY/DSIN(PSI)**2                                AMB1183
PSIN=PAI2-DATAN(COTN)                                         AMB1184
DPSI=PSIN-PSI                                         AMB1185
IF(DABS(DPSI).LT.1.D-6) GO TO 11                                AMB1186
1 CONTINUE                                         AMB1187
PRINT 12,I,ITER,PSI,PSIN,DPSI,M,XP,YP,T                         AMB1188
12 FORMAT(/1X,'I,ITER,PSI,PSIN,DPSI,M,XP,YP,T='//                AMB1189
1           1X,2I4,7D11.3/)                                         AMB1190
CALL SOF('2301')                                         AMB1191
11 CONTINUE                                         AMB1192
C USING MOB=M AS COMPUTED FROM THE INVERSE PROBLEM, FIND MAB.      AMB1193
MOB=M                                         AMB1194
CALL MFUNC(M,F,ETALF,TETA)                                         AMB1195
PSI=TETA+DASIN(1.D0/M)                                         AMB1196
CALL HINTER(M,HM)                                         AMB1197
GOREM=1.D0+G1*M**2                                         AMB1198
GOR=M**2-1.D0                                         AMB1199
DELTOB=0.5D0*DSQRT(GOR)*(1.D0/(MEXIT*ETALF))                     AMB1200
1           +DSIN(TETA)/M)/DSIN(PSI)+G15*HM/2.D0                  AMB1201
FOB=(G7*GOREM)**G2/M                                         AMB1202
FAB=FOB*(YP/YCOR)**DELTOB                                     AMB1203
CALL AREA(FAB,MAB)                                         AMB1204
EPSI0B=DELTOB/DSQRT(GOR)-DSIN(TETA)/(M*DSIN(PSI))                 AMB1205
KAPA0B=1.D0                                         AMB1206
IF(DABS(PAI2-TETA).GT.1.D-8)                                         AMB1207
1 KAPA0B=DTAN(TETA)*EPSI0B                                         AMB1208
COSTAB=DCOS(TETA)*(YP/YCOR)**(-KAPA0B)                           AMB1209
TETAAB=DACOS(COSTAB)                                         AMB1210
100 CONTINUE                                         AMB1211
RETURN                                         AMB1212
END                                         AMB1213
SUBROUTINE AREA(F,M)                                         AMB1214
C SUBROUTINE NUMBER 24                                         AMB1215
IMPLICIT REAL*8(A-H,O-Z,$)                                         AMB1216
REAL*8 MEXIT,MIN,M,MHINV                                         AMB1217
COMMON /GAMA/G,G1,G2,G3,G4,G5,G6,G7,G8,G9,G10,G11,G12,G13,G14,G15,AMB1218
1           G16,G17,G18,G19,G20                                         AMB1219
COMMON /PAR/C0,ENO,EM1,D,SIGMA,TLIM,DR0,ELO,Q0,T0,FACT,ALOGF,    AMB1220
1           DPSI0,DTMAX,DETA0,ETALIM,XSI,XSF                         AMB1221
COMMON /GRP/DMINV,MHINV(101),HMV(101)                                AMB1222
COMMON /IGRP/KHM                                         AMB1223
C COMPUTE MACH NUMBER M FROM AREA RATIO FUNCTION F                  AMB1224

```

```

C   F=((2/(G+1))*(1+(G-1)*M**2))**((G+1)/(2*(G-1)))/M          AMB1225
C   INITIAL GUESS IS MIN                                              AMB1226
  MEXIT=EM1
  E1=(F*MEXIT)**(1.D0/G2)/G7
  E2=(E1-1.D0)/G1
  E3=DMAX1(E2,MEXIT**2)
  MIN=DSQRT(E3)
  EMN=MIN
  DO 1 I=1,100
  EMO=EMN
  GOREM=1.D0+G1*EMO**2
  GOR=EMO**2-1.D0
  FO=(G7*GOREM)**G2/EMO
  DF=FO-F
C   PRINT 123,I,EMO,EMN,FO,F,DF,GOR,GOREM                         AMB1239
C123  FORMAT(1X,'I,EMO,EMN,FO,F,DF,GOR,GOREM=',I5,7D12.4)           AMB1240
  DFDM=FO*GOR/(EMO*GOREM)
  DMN=DF/DFDM
  EMN=EMO-DMN
  EPSEM=DABS(DMN/EMN)
  IF(EPSEM.LT.1.D-10) GO TO 11
1   CONTINUE
  CALL SOF('2401')
11  CONTINUE
  M=EMN
  RETURN
  END

```

8. DISTRIBUTION LIST	No. of Copies
1. Defense Technical Information Center Cameron Station Alexandria, VA 22314	2
2. Library, Code 0142 Naval Postgraduate School Monterey, CA 93943-5100.	2
3. Department Chairman, Code 67 Department of Aeronautics Naval Postgraduate School Monterey, CA 93943-5100.	1
4. Distinguished Professor Allen E. Fuhs Space Systems Academic Group, Code 72 Naval Postgraduate School Monterey, CA 93943-5100.	5
5. Dr. Neil Griff SDIO/DEO Washington, DC 20301-7100.	3
6. Mr. Bruce Pierce SDIO/DEO Washington, DC 20301-7100.	1
7. Dr. Joseph Falcovitz (24) Rafael Ballistic Center P. O. Box 2250 , Haifa Israel	5

	No. of Copies
8. Professor Oscar Biblarz Department of Aeronautics, Code 67 Naval Postgraduate School Monterey, CA 93943-5100.	1 ¹⁷
9. Research Administration Office Code 012 Naval Postgraduate School Monterey, CA 93943-5100.	1
10. Dr. P. Avizonis Air Force Weapons Laboratory Kirtland Air Force Base, NM 87117	1
11. Dr. John Lawless Space Power Inc. 1977 Concourse Drive San Jose, CA 95131	1
12. Dr. Mark Thornton Boeing Aerospace Company Post Office Box 3999 Seattle, WA 98124-2499	1
13. LT. Mark Price AFRPL Edwards AFB, CA 93523	1
14. Mr. Arthur W. Rogers Space Systems Division Hughes Aircraft Co. P. O. Box 92919, Los Angeles, CA 90009	1

No. of Copies

15.	LCOL Rick Babcock, USAF Air Force Geophysical Laboratory Hanscomb Field Bedford, MA 01730	1
16.	Mr. Ronald J. Hoffman Plume Technology and Spacecraft Contamination Division Science Applications International Co. 10000 Santa Monica Blvd., Suite 320 Los Angeles, CA 90067	1



DUDLEY KNOX LIBRARY



3 2768 00333301 4